

10/5/92 RSL 1395



1 Fairway Drive, Avalon
Lower Hutt 5010
PO Box 30368
Lower Hutt 5040
New Zealand
T +64-4-570 1444
F +64-4-570 4600
www.gns.cri.nz

Damage State Exceedance Probabilities from Aftershocks

M. C. Gerstenberger
N. Luco

S. R. Uma
H. Ryu

GNS Science Consultancy Report 2013/161
July 2013

DISCLAIMER

This report has been prepared by the Institute of Geological and Nuclear Sciences Limited (GNS Science) exclusively for and under contract to EQC. Unless otherwise agreed in writing by GNS Science, GNS Science accepts no responsibility for any use of, or reliance on any contents of this Report by any person other than EQC and shall not be liable to any person other than EQC, on any ground, for any loss, damage or expense arising from such use or reliance.

BIBLIOGRAPHIC REFERENCE

Gerstenberger, M. C.; Uma, S. R.; Luco, N.; Ryu, H. 2013. Damage State Exceedance Probabilities from Aftershocks, *GNS Science Consultancy Report 2013/161*. 43 p.

CONTENTS

NON-TECHNICAL ABSTRACT II
TECHNICAL ABSTRACT..... III

APPENDICES

**APPENDIX 1: A METHODOLOGY FOR POST-MAINSHOCK PROBABILISTIC
ASSESSMENT OF BUILDING COLLAPSE RISK 3**
**APPENDIX 2: DEVELOPING FRAGILITIES FOR MAINSHOCK-DAMAGED
STRUCTURES THROUGH INCREMENTAL DYNAMIC ANALYSIS 13**
**APPENDIX 3: COMPARISON OF MAIN-SHOCK AND AFTERSHOCK FRAGILITY
CURVES DEVELOPED FOR NEW ZEALAND AND US BUILDINGS..... 23**
**APPENDIX 4: AFTERSHOCK FRAGILITY CURVES AND TAGGING
ASSESSMENTS FOR A MAINSHOCK-DAMAGED BUILDING..... 33**

NON-TECHNICAL ABSTRACT

As demonstrated in the Canterbury earthquake sequence, shaking from aftershocks can be strong enough to cause significant damage and building collapse. This was a very specific case where in many locations the shaking from aftershocks was stronger than from the main shock; however, one important consideration is how vulnerable a building may become to aftershock shaking following shaking from a main shock. In this report we present a method for post-earthquake risk assessment for collapse of buildings.

Building on earlier work by Luco and others (Luco, et al., 2004; Yeo 2005), we extend the framework that is commonly used for probabilistic damage assessments prior to the occurrence of an earthquake. We start with the standard risk integral, which combines forecast ground motion hazard for a location (e.g., from the New Zealand National Seismic Hazard Model; NSHM) with building models that predict how much damage a given structure will experience from a specific level of ground shaking. By combining this information, a forecast of the level of building damage expected for a particular time frame can be calculated. Due to models such as the NSHM not taking account of shaking from aftershocks, we have used a method to include the potential for ground shaking from not only a main shock, but from possible aftershocks. Additionally, we have developed and included structural modelling that accounts for any possible damage from a main shock and then determines the potential for different levels of damage from subsequent shaking from aftershocks; the damage probabilities output from such modelling is typically referred to as building fragilities.

The two additional components we present in this work are, given a main shock: 1) forecast modelling of the possible aftershocks and their anticipated ground motions; and 2) building fragilities that include damage from the main shock and potential aftershocks. The aftershock modelling is handled with a model which accounts for families of aftershocks and forecasts the locations of expected aftershocks (i.e., the STEP model). We calculate the ground motions of the aftershocks using appropriate ground motion prediction equations, such as McVerry (2006) or Bradley (2010), for New Zealand. For the building damage modelling, we develop 4- and 5-story reinforced concrete frame computer models that represent a common building type in New Zealand. We then model the buildings using two levels of complexity: 1) in a simple approximation, the building is only allowed to move in one direction; and 2) in a more detailed model, the building is allowed to move in all directions. In both cases we model the response of the building to recorded ground motion observations for multiple main shocks and aftershocks. Using the results of this, we develop fragility curves that estimate the damage of the generic NZ structure from back-to-back shaking from a main shock and aftershock. When combined using the risk integral described above, we are then able to estimate the probability for building collapse given expected (or observed) main shocks and the potential for aftershocks. One key outcome is in a comparison with an equivalent U.S. reinforced concrete frame building where significant variability from the NZ model is observed; this indicates that the use of building models from other countries for developing building fragilities may be misleading.

TECHNICAL ABSTRACT

As demonstrated in the Canterbury earthquake sequence, shaking from aftershocks can be strong enough to cause significant damage and building collapse. Due to the locations of the events, this was a very specific case where, in many locations, the shaking from aftershocks was stronger than for the main shock; however, one important consideration is how vulnerable a building may become to aftershock shaking following shaking and damage from a main shock. In this report we present a method for post-earthquake probabilistic risk assessment for building collapse.

We extend existing work (e.g., Luco et al, 2004; Yeo, 2005) and develop a method that allows for a probabilistic estimate of the post-main shock risk that accounts for main shock induced structural damage and from the potential ground shaking and damage from subsequent aftershocks. The calculations are based on an extension of the standard risk integral equation where the necessary inputs are: 1) main shock ground motions, either observed or from a probabilistic forecast (e.g., using the New Zealand National Seismic Hazard Model; NSHM); 2) fragility functions for a structure of interest; 3) Expected ground motions from forecast aftershocks; and 4) fragility curves for the same structure calculated starting in all possible damage states from undamaged through to near collapse.

To model the aftershock component we use the STEP model (Gerstenberger et al, 2005) which models the expected aftershocks using super-imposed Omori sequences allowing for a spatially heterogeneous forecast. To model the ground-shaking hazard in New Zealand, we apply either the McVerry (2006) or Bradley (2010) ground motion prediction equation. The resulting forecast allows for a similar result to that of the NSHM, such as a grid of ground motion exceedance probabilities for a given return period.

We develop generic New Zealand structural models for 4- and 5-story reinforced concrete frame buildings. Treating these as either a SDOF(single-degree-of-freedom) or MDOF(multi-degree-of-freedom) oscillator, we subject the buildings to incremental dynamic analysis from back-to-back main shock and aftershock ground motions. First, fragility curves for various damage states (minor, moderate, severe, extensive and collapse) are derived under main shock ground motions. Next, we analyse the buildings under the various damage states to determine the probabilities of their collapse due to aftershocks.

Two main observations from this study are: (i) For a given class of building, there is a need to develop region-specific fragility curves and those available from overseas models are not suitable.; (ii) at a given ground motion intensity, the probability of collapse for a damaged building is higher than the probabilities of collapse for an undamaged building.

APPENDICES

This page is intentionally left blank.

APPENDIX 1: A METHODOLOGY FOR POST-MAINSHOCK PROBABILISTIC ASSESSMENT OF BUILDING COLLAPSE RISK



Proceedings of the Ninth Pacific Conference on Earthquake Engineering
 Building an Earthquake-Resilient Society
 14-16 April, 2011, Auckland, New Zealand

A methodology for post-mainshock probabilistic assessment of building collapse risk

N. Luco

Geologic Hazards Science Center, US Geological Survey (USGS), Golden, Colorado, USA.

M.C. Gerstenberger & S.R. Uma

GNS Science, Avalon, Lower Hutt, New Zealand.

H. Ryu, A.B. Liel & M. Raghunandan

Department of Civil Engineering, University of Colorado at Boulder, USA.

ABSTRACT: This paper presents a methodology for post-earthquake probabilistic risk (of damage) assessment that we propose in order to develop a computational tool for automatic or semi-automatic assessment. The methodology utilizes the same so-called risk integral which can be used for pre-earthquake probabilistic assessment. The risk integral couples (i) ground motion hazard information for the location of a structure of interest with (ii) knowledge of the fragility of the structure with respect to potential ground motion intensities. In the proposed post-mainshock methodology, the ground motion hazard component of the risk integral is adapted to account for aftershocks which are deliberately excluded from typical pre-earthquake hazard assessments and which decrease in frequency with the time elapsed since the mainshock. Correspondingly, the structural fragility component is adapted to account for any damage caused by the mainshock, as well as any uncertainty in the extent of this damage. The result of the adapted risk integral is a fully-probabilistic quantification of post-mainshock seismic risk that can inform emergency response mobilization, inspection prioritization, and re-occupancy decisions.

1 INTRODUCTION

1.1 Motivation

Increasingly, probabilistic seismic risk (of damage) assessment is becoming the basis for longer-term or “pre-earthquake” mitigation approaches for buildings and other structures, e.g. seismic design standards in building codes. For example, the latest edition of the American Society of Civil Engineers (ASCE) standard entitled “Minimum Design Loads for Buildings and Other Structures” (ASCE 2010) defines Risk-Targeted Maximum Considered Earthquake (MCE_R) ground motion maps for the United States (US) by explicitly targeting a probabilistic 1% risk of collapse in 50 years, an approximation of the lifespan of a building. These probabilistic risk-based maps have since been adopted for inclusion in the 2012 International Building Code (International Code Council 2012). Moreover, the next generation of performance-based seismic design procedures for new and existing buildings being developed by the Applied Technology Council (<http://www.atcouncil.org/Projects/atc-58-project.html>) use probabilistic risk of earthquake-caused deaths, dollars (repair costs), and downtime (repair duration) as metrics for seismic performance assessment of buildings.

1.2 Previous work

Probabilistic risk assessment has also been proposed as a basis for making shorter-term or “post-earthquake” mitigation decisions after a mainshock has occurred and when the threat of aftershocks

lingers. For example, the Advanced Seismic Assessment Guidelines developed by Bazzurro et al (2006) use the probability that an aftershock ground motion will exceed the capacity of a mainshock-damaged building (treated deterministically for simplicity) as a rational criterion for deciding whether and when to permit re-occupancy of the building. Similarly, Yeo & Cornell (2005) have developed a time-dependent building “tagging” (i.e. permitting or restricting occupancy) policy for the aftershock environment using probability of collapse as a proxy for fatality risk.

1.3 Preview of methodology

This paper presents the methodology for post-mainshock probabilistic risk assessment that we propose in order to develop a computational tool for automatic (or semi-automatic) assessment, with funding from the New Zealand Earthquake Commission (EQC). The methodology utilizes the same so-called risk integral (e.g., Applied Technology Council 1978, McGuire 2004) that can be used for pre-earthquake probabilistic risk assessment. As reviewed in Section 2 of the paper, the risk integral couples (i) ground motion hazard information for the location of a structure of interest with (ii) knowledge of the fragility of the structure with respect to potential ground motion intensities. In other words, the risk integral combines information about both the ground motion *demand* and the *capacity* of the structure to withstand such demand.

In the proposed post-mainshock methodology, explained in Section 3, the ground motion hazard/demand component of the risk integral is adapted to account for aftershocks which are deliberately excluded from typical pre-earthquake hazard assessments. Correspondingly, the structural fragility/capacity component is adapted to account for any damage caused by the mainshock, as well as any uncertainty in the extent of this damage. The result of the adapted risk integral is a fully-probabilistic quantification of the post-mainshock seismic risk, i.e. the risk of further damage in aftershocks. By comparing it with tolerated pre-earthquake risk levels (e.g. the 1%-in-50-years risk of collapse mentioned above in Section 1.1), the post-mainshock result can inform emergency response mobilization, inspection prioritization, and re-occupancy decisions, as discussed in Section 4.

1.4 Applications addressed in this paper

Although we focus on mainshock-aftershock sequences in this paper, the post-earthquake risk assessment methodology presented can be applied after any earthquake (a mainshock, aftershock, or foreshock). Furthermore, to the extent that the post-earthquake ground motion hazard component of the assessment includes the potential for so-called triggered earthquakes, the methodology can apply for sequences like the 1811-1812 New Madrid Seismic Zone earthquakes in the US and the recent 2010-2011 earthquakes near Christchurch in New Zealand (NZ).

We also focus on buildings in this paper, but analogous methodologies can be applied to other structures such as bridges and dams. While we focus on collapse risk in the sections that follow, the risk of exceeding any other state of damage can be considered with the same methodology.

2 PRE-MAINSHOCK RISK ASSESSMENT METHODOLOGY

2.1 Risk integral

Before a mainshock has occurred, and long enough after a past mainshock that the remaining threat of aftershocks is negligible, the risk of collapse of a building at a particular location can be computed via the risk integral mentioned above. As an early example, the risk integral was used in ATC 3-06 (Applied Technology Council 1978) to compute collapse risks that result from designing buildings for uniform-hazard ground motions. Recently, the risk integral has been used to revisit these ATC 3-06 computations (Luco et al 2007), and ultimately to derive the new MCE_R ground motions in (ASCE 2010) and FEMA P-750 (Building Seismic Safety Council 2009).

As expressed in Equation 1 for collapse risk, $\lambda[\text{Collapse}]$, the risk integral combines a collapse fragility curve for the building of interest, $\Pr[\text{Collapse}|IM=a]$, with a ground motion hazard curve for its location, $\lambda[IM>a]$. The fragility and hazard curve are described in more detail in the next two

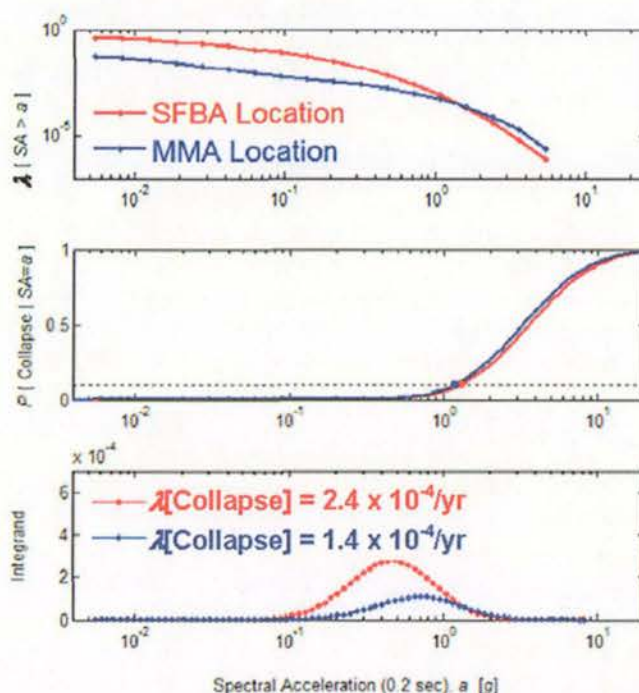


Figure 1. Illustration of the risk integral for computing collapse risk (bottom panel) via convolution of a collapse fragility curve (middle panel) with a ground motion hazard curve (top panel). The red and blue curves are for San Francisco Bay Area (SFBA) and Memphis Metropolitan Area (MMA) building locations, respectively. Each integrand curve in the bottom panel shows the product, at each ground motion intensity measure value (0.2-second spectral acceleration in this case), of the corresponding hazard curve and the derivative of the corresponding fragility curve. The area under (i.e. the integral of) each integrand curve is the collapse risk, i.e. the mean annual frequency of collapse. This figure has been adapted from (Luco et al 2007).

subsections, but in short (and loosely speaking) the fragility curve provides “what-if” probabilities of collapse for a range of potential ground motion intensity measure (IM) values, and the hazard curve provides annual probabilities of exceeding those IM values. The combination of these curves via the risk integral yields the annual (i.e. in-the-next-year) probability of collapse of the building at its particular location. Figure 1 illustrates the risk integral for two example buildings.

$$\lambda[\text{Collapse}] = \int_0^{\infty} \text{Pr}[\text{Collapse} | \text{IM} = a] \left| \frac{d\lambda[\text{IM} > a]}{da} \right| da \quad (1)$$

In Equation 1, λ is used in denoting the collapse risk and the ground motion hazard curve because, strictly speaking, both are in terms of mean annual frequency rather than annual probability. Probabilities for other time horizons (e.g. 50 years) are commonly calculated using a Poisson probability distribution (e.g. see McGuire 2004).

2.2 Collapse fragility curves

As illustrated in the middle panel of Figure 1, a collapse fragility curve summarizes the probability of collapse of a building for each in a range of IM values it could be subjected to. The probability is near-zero when the IM value is relatively small, and near-unity for a relatively large IM value.

A collapse fragility curve can be developed via expert opinion, data from past earthquakes and shake table experiments, and/or computer simulations. As will be explained below in Section 3.1, for our post-mainshock risk assessment methodology we develop the collapse fragility curve via (predominantly) computer simulations, namely nonlinear response history analyses (more specifically, incremental dynamic analyses) of a building model subjected to numerous ground motion seismograms. Such analyses are already being used to derive collapse fragility curves for *pre-*

mainshock risk assessment, e.g. in FEMA P-695 (ATC 2009) and (Ryu et al 2011). In the former, the collapse fragility curves derived are for specific multi-degree-of-freedom building models, whereas in the latter they are for generic single-degree-of-freedom building models that each represent a general type of building, e.g. a mid-rise reinforced concrete moment-resisting frame building. Both and other kinds of collapse fragility curves can be used in the pre- and post-mainshock risk assessment methodologies described in this paper.

2.3 Ground motion hazard curves

As illustrated in the top panel of Figure 1, a ground motion hazard curve for a location summarizes the mean annual frequency (MAF) of exceeding each in a range of potential IM values. The MAF is relatively high for small IM values, and relatively low for large IM values.

In pre-mainshock hazard assessment, ground motion hazard curves are computed via Probabilistic Seismic Hazard Analysis (PSHA; Cornell 1968, McGuire 2004). PSHA combines information on potential sources of earthquakes (e.g. faults and locations of past earthquakes), potential magnitudes of earthquakes from these sources and their frequencies of occurrence, and potential ground motions generated by these earthquakes. Uncertainty and randomness in each of these components is accounted for in the combination. For a grid of locations covering the US, pre-mainshock hazard curves computed via PSHA are readily available from the USGS National Seismic Hazard Mapping Project (<http://earthquake.usgs.gov/hazards/products/>).

It is relevant to note that aftershocks (and foreshocks) are deliberately removed from the catalogues of historical earthquakes used for typical PSHA computations, in order to be consistent with the conventional assumption of independent (Poissonian) earthquakes in time, as opposed to mainshock-aftershock clusters. As will be summarized below in Section 3.3, we make use of an adapted version of PSHA in computing hazard curves for our *post*-mainshock risk assessment methodology.

3 POST-MAINSHOCK RISK ASSESSMENT METHODOLOGY

3.1 "Post-earthquake risk integral"

As alluded to above in the introduction, after a mainshock the risk of a building at a particular location collapsing in an aftershock can still be computed via the risk integral (Equation 1). If the building *was not* damaged by the mainshock, the only change is that the ground motion hazard curve used in the risk integral is now one that accounts for the threat of aftershocks. The aftershock hazard decreases with the time elapsed since the mainshock, however, rapidly enough that the aftershock hazard curves we use are expressed in terms of a 24-hour time period (Gerstenberger et al 2004). As a result, our "post-earthquake risk integral" computes daily probabilities (strictly speaking, mean daily frequencies) of collapse, instead of the annual probabilities commonly computed in pre-mainshock use of the risk integral. Longer post-mainshock time horizons that account for the time-varying aftershock hazard can be considered via "equivalent constant rates" proposed by Yeo & Cornell (2005).

If the building *was* damaged (but not already collapsed) by the mainshock, not only is the hazard curve used in the risk integral changed, but so is the fragility curve. The substituted fragility curve accounts for the damage caused by the mainshock, as well as any uncertainty in the extent of this damage. Our methodology for deriving such post-mainshock fragility curves is discussed in the next subsection and in the PCEE 2011 paper by Ryu et al (paper number 225).

3.2 Post-mainshock fragility curves

As one might expect, the fragility curves used in our post-mainshock risk assessment methodology account for any damage caused by the mainshock. This typically increases the probabilities of collapse for the considered range of potential (future) IM values, as illustrated in Figure 2. The amount of increase depends of course on the extent of the mainshock damage, which is commonly discretized into so-called damage states, e.g. none, slight, moderate, extensive, and complete in HAZUS, the US Federal Emergency Management Agency (FEMA) methodology for estimating potential losses from disasters (<http://www.fema.gov/hazus/>). As will be explained below, uncertainty in what damage state

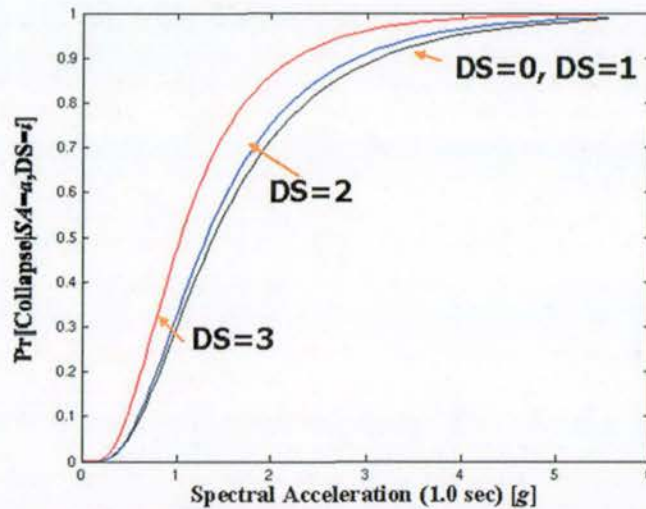


Figure 2. Example damaged-building fragility curves for certain damage states caused by the mainshock. The damage states are no damage (DS=0), onset of nonlinear behaviour in the building (DS=1), fracture of exterior beam-column connections in the first floor (DS=2), and fracture of interior connections (DS=3). As explained in the paper, if the actual damage state is uncertain (e.g. before inspection), the various fragility curves are averaged with weights corresponding to the probability of each possible post-mainshock damage state. This figure has been adapted from (Gerstenberger et al 2008).

resulted from the mainshock, e.g. due to incomplete inspection, is accounted for in our post-mainshock fragility curves.

For a certain (given) damage state caused by the mainshock, we develop a corresponding damaged-building fragility curve with a procedure proposed in (Ryu et al 2011), which is an improvement of the procedure in (Luco et al 2004). Very briefly, the procedure first generates numerous realizations of the building in the given damage state via nonlinear response history analyses (more specifically, incremental dynamic analyses) of the originally undamaged building model using numerous seismograms that represent mainshock ground motions. While the broad damage state (e.g., “moderate”) is the same for each realization, the details of the state of the building are different for each realization, and the numerous realizations sample these differences. Then a fragility curve is developed for each realization of the damaged building, again via nonlinear response history analyses (incremental dynamic analyses), but now of the damaged-building model. The seismograms used in these damaged-building analyses represent aftershock ground motions (although they do not necessarily need to be recordings from aftershocks exclusively). Finally, the fragility curves for the numerous realizations are, in effect, averaged to arrive at the fragility curve for the given damage state of interest.

Uncertainty in the extent of any mainshock damage – i.e., uncertainty in the “post-mainshock damage state” – is accounted for in our methodology by applying the theorem of total probability. As expressed in Equation 2, the post-mainshock fragility curve, $\Pr[\text{Collapse}|\text{IM}=a]$, is equal to a weighted average of the fragility curves for all of the n possible post-mainshock damage states, each denoted $\Pr[\text{Collapse}|\text{IM}=a, \text{DS}=i]$. The respective weights are the probabilities of the possible post-mainshock damage states, $\Pr[\text{DS}=i]$, which can be determined in the three different ways that are discussed in the next three subsections.

$$\Pr[\text{Collapse} | \text{IM} = a] = \sum_{i=1}^n \Pr[\text{Collapse} | \text{IM} = a, \text{DS} = i] \Pr[\text{DS} = i] \quad (2)$$

3.2.1 ShakeMap-based post-mainshock damage state probabilities

Promptly after an earthquake, a ShakeMap (e.g. from <http://earthquake.usgs.gov/shakemap/>) provides best-estimates of ground motion IM values experienced, typically based on (i) a magnitude, location, and other information about the earthquake, (ii) information about the near-surface geology of the affected region, (iii) a ground motion prediction equation like the Next Generation Attenuation (NGA) relationships for the Western US (<http://peer.berkeley.edu/ngawest/>), and (iv) if available, IM values from recording stations. A parallel map of the uncertainty in the IM values generated by the earthquake can also be produced, with no (or at most little) uncertainty at the recording stations. More formally, the maps provide a median and logarithmic standard deviation of the IM at each location, denoted here as m_{IM} and $\sigma_{\ln IM}$, respectively.

With m_{IM} and $\sigma_{\ln IM}$ for the location of a building of interest, a lognormal complementary cumulative probability distribution of the IM value generated by the mainshock can be calculated according to Equation 3, where a denotes each in a range of possible IM values.

$$\Pr[IM > a] = 1 - \Phi \left[\frac{\ln a - \ln m_{IM}}{\sigma_{\ln IM}} \right] \quad (3)$$

In order to propagate the IM probability distribution in Equation 3 into post-mainshock damage state probabilities, we slightly modify the components of the risk integral given in Equation 1. More specifically, we couple the ShakeMap-based IM probability distribution, $\Pr[IM > a]$, with a fragility curve for the pre-mainshock (or undamaged) building and the damage state of interest, $\Pr[DS > i | IM = a]$. This combination is expressed mathematically in Equation 4.

$$\Pr[DS > i] = \int_0^{\infty} \Pr[DS > i | IM = a] \left| \frac{d\Pr[IM > a]}{da} \right| da \quad (4)$$

The post-mainshock damage state probabilities, $\Pr[DS=i]$, are then calculated by using Equation 4 for both the damage state of interest (e.g., “moderate”) and the next greater damage state (e.g. “severe”), i.e. $\Pr[DS=i] = \Pr[DS > i] - \Pr[DS > i+1]$. Note that these automatable post-mainshock damage state probabilities can themselves inform emergency response mobilization, when applied to an inventory of structures. Though not via the fully-probabilistic Equation 4, the USGS ShakeCast application (<http://earthquake.usgs.gov/shakecast/>) delivers such information that is already used for emergency response purposes in the US. Via Equation 4 and the ShakeMap system currently being developed for NZ, our computational tool will also deliver such intermediate (to post-earthquake risk) information.

3.2.2 Inspection-based post-mainshock damage state probabilities

A post-mainshock inspection of a building by a structural engineer can improve upon the prompt ShakeMap-based damage state probabilities described in the preceding subsection. For example, the engineer might opine that the observed damage is fully consistent with the damage state “2” defined in the caption of Figure 2 (i.e. $\Pr[DS=2]=1$), or that it may be indicative of damage states 2 or 3, with equal likelihood (i.e. $\Pr[DS=2]=\Pr[DS=3]=0.5$). In fact, the engineer could be asked to assign likelihoods for all of the discrete damage states identified (e.g., $\Pr[DS=0]=0$, $\Pr[DS=1]=0.1$, $\Pr[DS=2]=0.6$, $\Pr[DS=3]=0.3$). Note that this allows the engineer to first focus on the state of damage of the building, rather than the more subjective re-occupancy decision. The collapse risks that result from inputting $\Pr[DS=i]$ into Equation 2 and ultimately the risk integral (Equation 1) can subsequently inform the re-occupancy decision.

3.2.3 Building-instrumentation-based post-mainshock damage state probabilities

Although not discussed in detail in this paper, building instrumentation data (e.g. peak transient and/or residual roof displacements) from a mainshock can be used to determine or constrain post-mainshock damage state probabilities. For example, residual roof displacement observations can be coupled with results from the nonlinear response history analyses conducted to develop pre-mainshock fragility curves (see Section 2.2). This coupling can be accomplished via a Bayesian updating methodology.

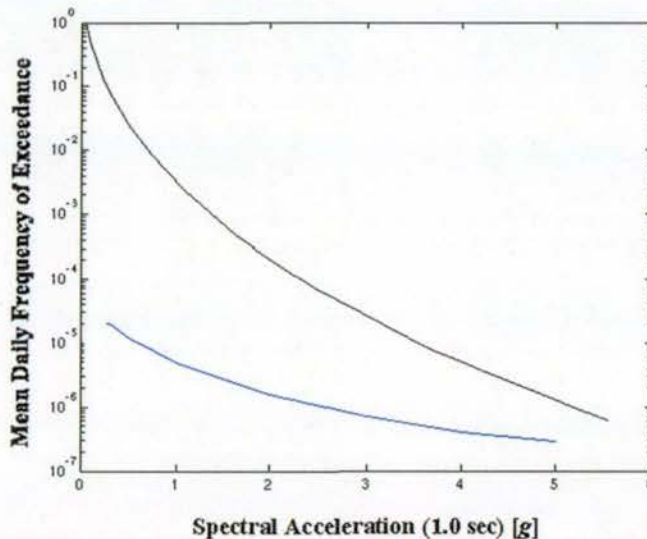


Figure 3. Example aftershock ground motion hazard curve (upper line) at a location 10km from the 1994 Northridge, California mainshock (magnitude 6.7), immediately after the earthquake. For comparison, the pre-mainshock hazard curve (lower line) for the same location is also shown. This figure has been adapted from (Gerstenberger et al 2008).

3.3 Aftershock ground motion hazard curves

Post-mainshock, ground motion hazard curves that account for potential aftershocks can be computed via an adaptation of pre-mainshock PSHA (described in Section 2.3). The USGS and GNS Science 24-Hour Aftershock Forecast Maps for California (<http://earthquake.usgs.gov/earthquakes/step/>) and NZ (<http://www.geonet.org.nz/canterbury-quakes/aftershocks/>), respectively, provide one point for such hazard curves via the PSHA adaptation explained in (Gerstenberger et al 2004). Full aftershock ground motion hazard curves are being computed for NZ, in near-real time, as part of our development of a computational tool for post-earthquake risk assessment. The third iteration of the Uniform California Earthquake Rupture Forecast (see <http://www.wgcep.org/versions/>) plans to develop an operational earthquake forecast that could, in the future, be extended to provide full aftershock ground motion hazard curves as well. As demonstrated in Figure 3, an aftershock hazard curve can be orders of magnitude higher (on the frequency of exceedance scale) than its conventional pre-mainshock counterpart, particularly immediately after the mainshock.

4 CONCLUDING REMARKS

4.1 Summary of proposed methodology

The proposed methodology for post-earthquake probabilistic risk assessment utilizes the same so-called risk integral that can be used for pre-earthquake probabilistic assessment. The risk integral couples i) ground motion hazard information for the location of a structure of interest with ii) knowledge of the fragility of the structure with respect to potential ground motion intensities. In the proposed post-mainshock methodology, the ground motion hazard component of the risk integral is adapted to account for aftershocks which are deliberately excluded from typical pre-earthquake hazard assessments and which decrease in frequency with the time elapsed since the mainshock. Correspondingly, the structural fragility component is adapted to account for any damage caused by the mainshock, as well as any uncertainty in the extent of this damage.

4.2 Examples of potential applications

The results of the proposed probabilistic post-earthquake risk assessment methodology can inform emergency response mobilization, inspection prioritization, and re-occupancy decisions. More

specifically, the intermediate post-mainshock damage state probabilities computed via Equation 4 for an inventory of buildings can be used in deciding where to send emergency response teams – e.g. wherever the probability is high that the post-mainshock damage state is collapse. Similarly, the post-mainshock collapse risks computed via the post-earthquake risk integral described in Section 3 can be used in prioritizing inspections of buildings that did not collapse in the mainshock but have a high risk of collapsing in an aftershock or “triggered” earthquake. The eventual inspections of individual buildings can also make use of the post-mainshock collapse risks, in making re-occupancy (e.g. red/yellow/green tag) decisions by comparing against corresponding pre-mainshock collapse risks. Note that by making use of the post-mainshock collapse risks, the re-occupancy decisions can (if desired) change with the time elapsed since the mainshock, as the frequency of aftershocks decreases and hence so do the post-mainshock collapse risks.

5 ACKNOWLEDGEMENTS

Our development of a computational tool for automatic/semi-automatic post-earthquake probabilistic risk assessment is funded by (i) the EQC Biennial Grants Programme 2010 (project 10/592), (ii) a cooperative agreement with the University of Colorado at Boulder funded by the USGS (award number G10AC00100), and (iii) in-kind research efforts from GNS Science, the University of Colorado at Boulder, and the USGS.

This paper was reviewed by Prof. John van de Lindt of The University of Alabama, Dr. Edward Field of the USGS, and Mr. David Perkins of the USGS. We sincerely appreciate their comments.

REFERENCES

- American Society of Civil Engineers 2010. *Minimum Design Loads for Buildings and Other Structures, ASCE/SEI 7-10*. Reston, Virginia: ASCE.
- Applied Technology Council 1978. *Tentative Provisions for the Development of Seismic Regulations for Buildings, ATC 3-06*. Palo Alto, California: ATC.
- Applied Technology Council 2009. *Quantification of Building Seismic Performance Factors, FEMA P-695*. Washington, DC: Federal Emergency Management Agency.
- Bazzurro, P., Cornell, C.A., Menun, C., Motahari, M. & Luco, N. 2006. *Advanced Seismic Assessment Guidelines, PEER Report 2006/05*. Berkeley, California: Pacific Earthquake Engineering Research Center.
- Building Seismic Safety Council 2009. *NEHRP Recommended Seismic Provisions for New Buildings and Other Structures, FEMA P-750*. Washington, DC: Federal Emergency Management Agency.
- Cornell, C.A. 1968. Engineering Seismic Risk Analysis, *Bulletin of the Seismological Society of America*, 58(5): 1583-1606.
- International Code Council 2012. *International Building Code*. Falls Church, Virginia: ICC.
- Luco, N. B.R. Ellingwood, R.O. Hamburger, J.D. Hooper, J.K. Kimball & Kircher, C.A. 2007. Risk-Targeted versus Current Seismic Design Maps for the Conterminous United States. *Proceedings of the Structural Engineers Association of California 76th Annual Convention*.
- McGuire, R.K. 2004. *Seismic Hazard and Risk Analysis*. Oakland, California: EERI.
- Ryu, H., Luco, N., Uma, S.R. & Liel, A.B. 2011. Developing fragilities for mainshock-damaged structures through incremental dynamic analysis. *9PCEE Paper No. 225*.
- Ryu, H., Luco, N. & Baker, J.W. 2011. Collapse Fragility Curves for Generic Building Types. In preparation for publication in *Earthquake Spectra*.
- Yeo, G.L. & Cornell, C.A. 2005. *Stochastic Characterization and Decision Bases under Time-Dependent Aftershock Risk in Performance-Based Earthquake Engineering, PEER Report 2005/13*.
- Gerstenberger, M., Wiemer, S. & Jones, L. 2004. *Real-time Forecasts of Tomorrow's Earthquakes in California: A New Mapping Tool, USGS Open-File Report 2004-1390*.
- Gerstenberger, M., Uma, S.R. & Luco, N. 2008. Calculation of damage state exceedance probabilities from aftershocks. *2008 NZSEE Conference Poster*.

This page is intentionally left blank.

**APPENDIX 2: DEVELOPING FRAGILITIES FOR MAINSHOCK-DAMAGED
STRUCTURES THROUGH INCREMENTAL DYNAMIC ANALYSIS**



Proceedings of the Ninth Pacific Conference on Earthquake Engineering
 Building an Earthquake-Resilient Society
 14-16 April, 2011, Auckland, New Zealand

Developing fragilities for mainshock-damaged structures through incremental dynamic analysis

H. Ryu

University of Colorado at Boulder, Boulder, CO USA. (now Geoscience Australia, Canberra, ACT Australia)

N. Luco

US Geological Survey, Golden, CO USA.

S. R. Uma

GNS Science, Avalon, Lower Hutt, New Zealand.

A. B. Liel

University of Colorado at Boulder, Boulder, CO USA.

ABSTRACT: We present a methodology for developing fragilities for mainshock-damaged structures, “aftershock fragility”, by performing incremental dynamic analysis (IDA) with a sequence of mainshock-aftershock ground motions. The aftershock fragility herein is distinguished from a conventional fragility for an intact structure. We estimate seismic response of a mainshock-damaged building by performing nonlinear time history analysis with a sequence of mainshock and aftershock ground motions (so-called “back-to-back” dynamic analysis). We perform the back-to-back dynamic analyses for a number of levels of mainshock response/damage, and a number of sequences of mainshock and aftershock ground motions. With estimated seismic responses from the back-to-back dynamic analyses, we compute various damage state transition probabilities, the probability of exceeding a higher damage state from an aftershock given a damage state due to a mainshock. For an illustration of the methodology, we develop an aftershock fragility for a typical New Zealand 5-storey reinforced concrete moment frame building. The building is modeled using a single-degree-of-freedom (SDOF) damped nonlinear oscillator with force-deformation behavior represented by a multi-linear capacity/pushover curve with moderate pinching hysteresis and medium cyclic deterioration.

1 INTRODUCTION

Most of current seismic risk assessment tools consider risk due to a mainshock event only. However, it is common to observe many aftershocks following the mainshock event, some of which could be strong enough to cause further damage to the building and even loss of human life. After a major earthquake, structural engineers must assess whether damaged buildings can continue to be occupied or not, with due consideration to the threat of aftershocks. An objective and quantifiable criterion that can be used to green/yellow/red-tag a damaged building (within a specified time period) is the probability of collapse in an aftershock. The probability of collapse in an aftershock can be computed by coupling the fragility of mainshock-damaged building with the aftershock ground motion hazard at the location.

Luco et al., (2004) proposed a methodology to compute the residual capacity of a mainshock-damaged building, which could be adopted to develop a fragility for a mainshock-damaged building. In the methodology, the residual capacity of a building in a given post-mainshock damage state is defined as

the smallest ground motion spectral acceleration that would induce localized or complete collapse in an aftershock. Each of five post-mainshock damage states is defined by a deterministic value of peak roof drift. For each realization of a mainshock-damaged building, residual capacities are computed by performing incremental dynamic analysis with aftershock records. There are two major limitations in this methodology: 1) the post-mainshock response given the post-mainshock damage state was assumed to be deterministic; 2) the damage state threshold was assumed to be deterministic.

In this study, we present a methodology for developing fragilities for mainshock-damaged structures, “aftershock fragilities”, by performing incremental dynamic analysis (IDA) with a sequence of mainshock-aftershock ground motions. More specifically, we estimate seismic response of a mainshock-damaged building by performing nonlinear time history analysis with a sequence of mainshock and aftershock ground motions (so-called “back-to-back” dynamic analyses). We perform the back-to-back dynamic analyses for a number of levels of mainshock response/damage, and a number of sequences of mainshock and aftershock ground motions. With estimated seismic responses from the back-to-back dynamic analyses, we compute various damage state transition probabilities, the probability of exceeding a higher damage state in an aftershock given a damage state caused by a mainshock. For an illustration of the methodology, we develop an aftershock fragility for a typical New Zealand 5-storey reinforced concrete moment frame building. The building is modeled using a single-degree-of-freedom (SDOF) damped nonlinear oscillator with force-deformation behavior represented by a multi-linear capacity/pushover curve with moderate pinching hysteresis and medium cyclic deterioration.

2 METHODOLOGY

In this section, we present the methodology for developing fragilities for a mainshock-damaged building. We first describe how fragility curves for an intact building are developed, and then describe the methodology for developing fragilities for a mainshock-damaged building.

2.1 Fragility for intact building

A building fragility curve defines the probability that a building experiences a certain damage state or worse, as a function of ground motion intensity. Fragility curves can be computed following Equation 1:

$$P(DS \geq ds | IM = im) = \int P(DS \geq ds | EDP = edp) \times f(EDP = edp | IM = im) dedp \quad (1)$$

where DS denotes damage state (e.g., slight), IM denotes ground motion intensity (e.g., spectral acceleration), and EDP denotes engineering demand parameter (e.g., drift). The first term in Equation 1, $P(DS \geq ds | EDP = edp)$, represents the probability of being in or exceeding a damage state, ds , given edp , and can be computed as

$$P(DS \geq ds | EDP = edp) = P(DST_{ds} \leq edp) \quad (2)$$

where DST_{ds} represents the damage state threshold (or capacity). The second term, $f(edp | im)$, represents the probability distribution of engineering demands on the structure for a specified ground motion intensity level and can be computed using the results of dynamic analysis of the building under a large number of ground motion records (e.g., incremental dynamic analyses).

Equation 1 can be rewritten as shown in Equation 3:

$$P(DS \geq ds | IM = im) = \int P(IM_{ds} \leq im | DST_{ds} = edp) \times f(DST_{ds} = edp) dedp \quad (3)$$

where IM_{ds} represents the capacity for damage state ds in terms of ground motion intensity (IM). The left-hand integrand in Equation 3 represents the probability that the ground motion intensity of interest, im , exceeds the capacity for the damage state, and can be computed using the distribution of

ground motion intensities causing a particular edp level. The right-hand integrand, $f(DST_{ds} = edp)$, can be computed using the defined damage state threshold information for the damage state. Note that $P(DST_{ds} \leq edp)$ in Equation 2 is the cumulative distribution function (CDF) of DST_{ds} , while $f(DST_{ds} = edp)$ is the probability density function (PDF) of DST_{ds} . Equation 3 is useful due to practical difficulties in estimating $f(edp|im)$, mainly due to the fact that the edp is infinite or not available whenever im is larger than the collapse capacity intensity measure.

2.2 Fragility for mainshock-damaged building

The fragility for a mainshock-damaged building can be computed using Equation (4):

$$P(DS_a > ds_a | IM_a = im_a, DS_m = ds_m) = \int P(DS_a > ds_a | IM_a = im_a, EDP_m = edp_m) \times f(EDP_m = edp_m | DS_m = ds_m) d edp_m \quad (4)$$

where DS_a represents the post-aftershock damage state, DS_m represents the post-mainshock damage state, EDP_m represents the mainshock building response, and IM_a represents the ground motion intensity of an aftershock.

The first term in Equation 4, $P(DS_a > ds_a | IM_a = im_a, EDP_m = edp_m)$, can be computed using either Equation 1 or Equation 3 for a mainshock-damaged building whose mainshock response (EDP_m) is edp_m . The second term in Equation 4, $f(EDP_m = edp_m | DS_m = ds_m)$, can be computed using the assumed distribution of mainshock response given post-mainshock damage state. In reality, the integral over the continuous range of mainshock response is replaced with summation over discrete levels of mainshock response.

If we assume a deterministic mainshock response given the post-mainshock damage state, then

$$P(DS_a > ds_a | IM_a = im_a, DS_m = ds_m) = P(DS_a > ds_a | IM_a = im_a, EDP_m = mDST_{ds,m}) \quad (5)$$

where $mDST_{ds,m}$ is the mainshock response for the given post-mainshock damage state.

Furthermore, if we assume no uncertainty in the damage state threshold, then

$$P(DS_a > ds_a | IM_a = im_a, DS_m = ds_m) = P(IM_{a,ds} < im_a | DST_{ds} = mDST_{ds,a}, EDP_m = mDST_{ds,m}) \quad (6)$$

where $mDST_{ds,a}$ is the deterministic damage state threshold for post-aftershock damage.

3 ILLUSTRATION

For an illustration of the proposed methodology, we have developed fragilities for a typical mid-rise concrete moment resisting frame structure in New Zealand.

3.1 Building simulation model

For the numerical model, we chose a SDOF model that represents the typical mid-rise concrete moment resisting frame structure in New Zealand. The derivation of a multilinear capacity curve for the model is explained in detail in Ryu et al. (2008) and Uma et al. (2011). Figure 1 shows the capacity curve of the model along with the median damage state threshold for five damage states (Slight, Moderate, Extensive, Complete and Collapse). The logarithmic standard deviation of each damage state threshold was set to 0.4. To simulate the nonlinear hysteretic behavior of the model under dynamic loading, we assumed medium pinching ($\kappa_{f,d} = 0.5$) and medium levels of cyclic

deterioration ($\gamma_{s,d} = 50$ and $\gamma_k = 100$) (Ibarra, 2003). Figure 1b shows the hysteretic behavior of the model under cyclic static loading. The elastic damping ratio is 7%, chosen by taking the damping ratio of the midrise concrete moment frame (CIM) in the US-based HAZUS software (FEMA, 2003). The model has a vibration period of 1.3 seconds.

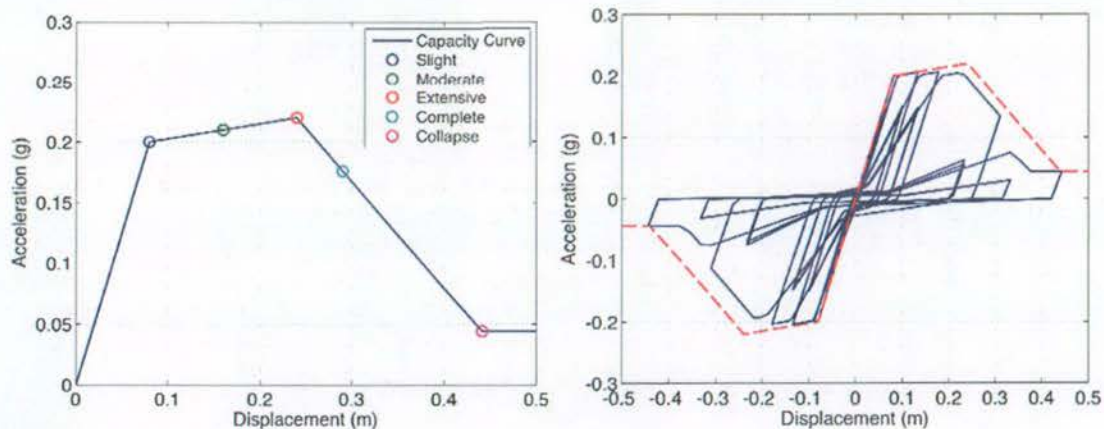


Figure 1 a) Capacity curve of the SDOF model; b) Hysteretic behavior of the model under static cyclic loading.

3.2 Ground motions

We used the suite of 30 records compiled by Vamvatsikos and Cornell (2006) for both mainshock and aftershock records. The moment magnitude for each of the records was within the range of 6.5 to 6.9, and the closest distance to fault rupture was within 15-33km. Spectral acceleration at 1.3 sec (i.e., the vibration period of the model) with a damping ratio of 5% was chosen as the ground motion intensity measure.

3.3 Fragility of an undamaged building

We performed IDA for a total of 30 mainshock records, and the resulting IDA curves are shown in Figure 2a. Using Equation 3, we computed the fragility of the undamaged building (i.e., the mainshock fragility) for each of the five damage states, including collapse, as shown in Figure 2b. The median and the logarithmic standard deviation of the collapse capacity of the undamaged building model are 0.86g and 0.42, respectively. Note that the *EDP* is the peak displacement of the SDOF model experienced during the earthquake.

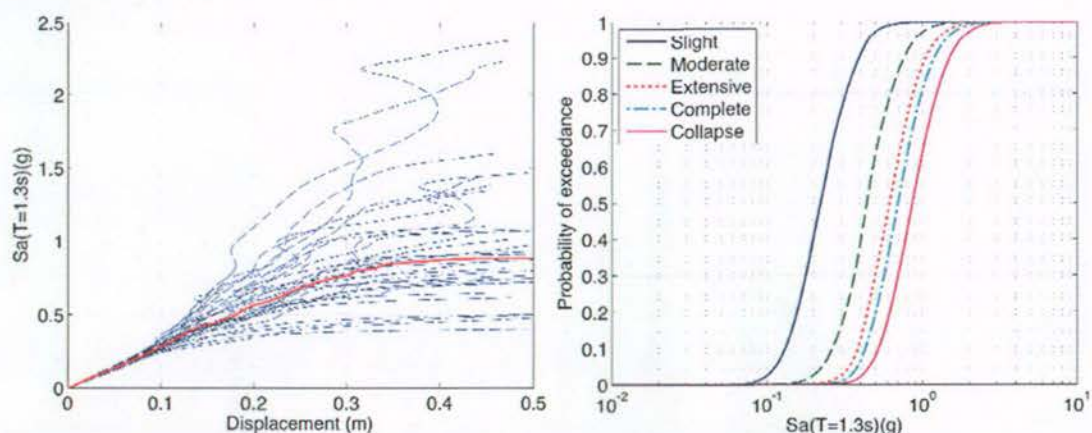


Figure 2 a) IDA curves for the undamaged building model; b) fragilities for the undamaged building model and the five potential damage states

3.4 Simulation of mainshock damage

In this paper, we focus on the collapse fragility (with respect to aftershocks) of the structure in the extensive damage state (due to a mainshock). The post-mainshock damage state is associated with the peak mainshock response. We have considered two different cases of a post-mainshock extensive damage state: 1) deterministic; the peak mainshock response is set equal to 0.24m, the median damage state threshold for the extensive damage state; 2) uncertain; the peak mainshock response is assumed to follow a lognormal distribution with 0.24m and 0.4 for the median and logarithmic standard deviation of the extensive damage state threshold, respectively.

In the case of the deterministic mainshock response, each mainshock record was scaled so that mainshock response was equal to 0.24m. In the case of the uncertain mainshock response, a similar approach may be applied; the process for the deterministic mainshock response was repeated for a number of sampled values representing the distribution of mainshock responses. Since it be too time-consuming to perform IDA for every possible value of mainshock response, we used Monte Carlo simulation instead, generating 30 values of mainshock response from the assumed distribution, and assigning each mainshock response to a mainshock record. Therefore the case of uncertain mainshock response is not different from the deterministic case in terms of computational effort.

3.5 Performing IDA with a sequence of mainshock and aftershock records

In order to perform IDA for a mainshock-damaged building, a sequence of mainshock and aftershock records was entered into the model. For a given sequence of mainshock and aftershock records, the scale factor for a given mainshock response was unchanged while the intensity of the aftershock record was scaled until the model collapsed.

Unlike the mainshock response, aftershock response can be different when the aftershock record is scaled by positive versus negative factors (to represent different polarities), because of residual drifts and damage in the mainshock-damaged building. In this study, we computed both aftershock responses by applying positive and negative factors to the aftershock records. Figure 3 shows two IDA curves where one is for the aftershock record scaled by positive factors and the other is for the aftershock record scaled by negative factors. Note that Luco et al. (2004) picked the smallest aftershock spectral acceleration that induced collapse for the residual collapse capacity. Similarly, we have used the polarity leading to the maximum aftershock response, as described below.

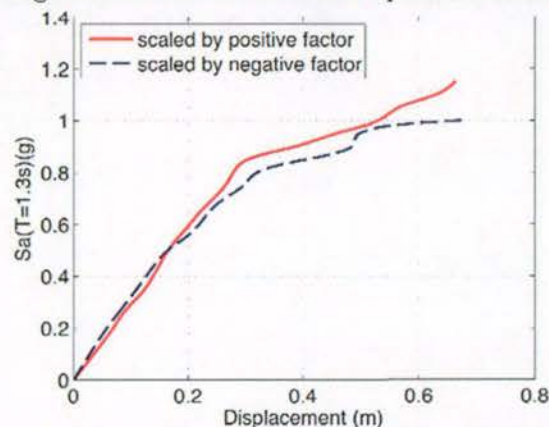


Figure 3 Comparison of two IDA curves: one is for an aftershock record scaled by positive factors, while the other is for an aftershock record scaled by negative factors.

The IDAs were performed using the OpenSees platform (McKenna and Fenves, 2000). Since IDAs over a sequence of mainshock and aftershock records require a large number of nonlinear dynamic analyses, the parallel version of OpenSees (OpenSeesMP) was run on a Linux cluster with multiple processors. The total number of dynamic analyses was the product of 30 (number of mainshock records), 30 (number of aftershock records), 2 (either positive or negative factors applied to aftershock

records), and the number of scale factors applied to each aftershock record until the model collapsed.

Figure 4a shows IDA curves for 30 sequences of various mainshock records and one aftershock record, whereas Figure 4b shows IDA curves for 30 sequences of one mainshock record and various aftershock records. As noted in Luco et al. (2004), there is relatively little variation with mainshock records of the aftershock response, since all the mainshock records are scaled to the considered level of mainshock response (in our case, for extensive damage).

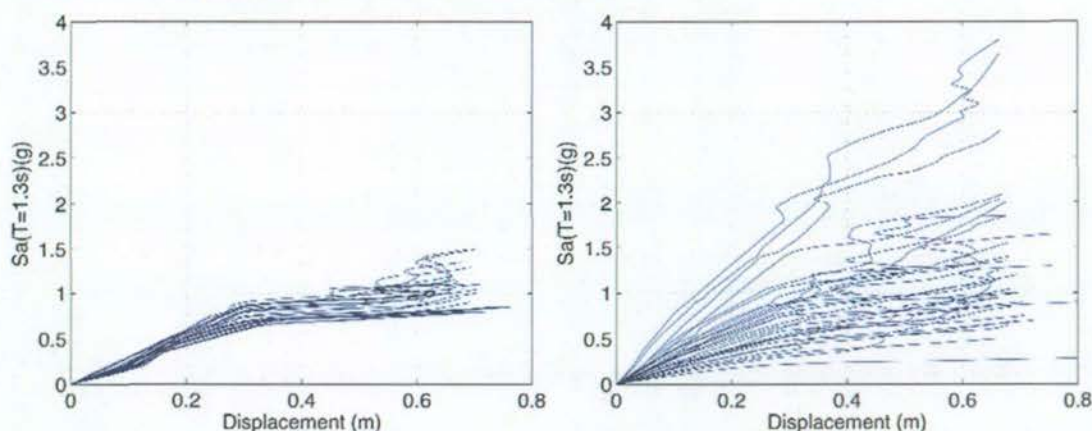


Figure 4 a) IDA curves for the sequences of various mainshock records and one aftershock record; b) IDA curves for the sequences of one mainshock record and various aftershock records.

3.6 Fragility of mainshock-damaged building

For the collapse damage state threshold, we have used either 1) a deterministic threshold, defined as 0.44m, the median damage state threshold for collapse, or 2) an uncertain threshold, defined by a lognormal distribution with 0.44m and 0.4 for the median and logarithmic standard deviation of the collapse damage state threshold, respectively.

First, we computed the collapse fragility of a mainshock-damaged building whose mainshock response was equal to a roof displacement 0.24m, using the deterministic collapse damage state threshold (see the Equation 5). Figure 5a shows three computed collapse fragility curves. As mentioned in the previous section, there were two aftershock responses depending on whether the aftershock record is scaled by positive or negative factors. In Figure 5a, the first curve was computed by choosing the maximum response between the positive and negative factors, the second curve was computed by choosing the minimum response between them, and the third curve was computed by choosing a response randomly between them. For this particular example, the differences among three cases are negligible. Hereafter, the collapse fragility computed using the maximum response will be used for comparison purpose.

Second, we computed the collapse fragility of a mainshock-damaged building whose mainshock response was equal to 0.24m, but with uncertainty in the 0.44m collapse threshold (see the Equation 4). The result is a negligible difference compared to the collapse fragility derived using the deterministic threshold, especially for lower levels of ground motion intensity.

Third, we computed the collapse fragility of a mainshock-damaged building whose mainshock response follows a lognormal distribution with 0.24m and 0.4 for the median and logarithmic standard deviation of the extensive damage state threshold, respectively, and with uncertainty in the collapse threshold (see the Equation 3).

All three of the computed collapse fragilities for a mainshock-damaged building are compared against the collapse fragility for the undamaged building in Figure 5b. The median collapse capacities of the mainshock-damaged building for three cases are 0.76g, 0.72g, and 0.72g, respectively. These represent decreases by approximately 16% from the median collapse capacity of 0.86g for the undamaged building. The reduction in the median collapse capacity is surprisingly small considering that the

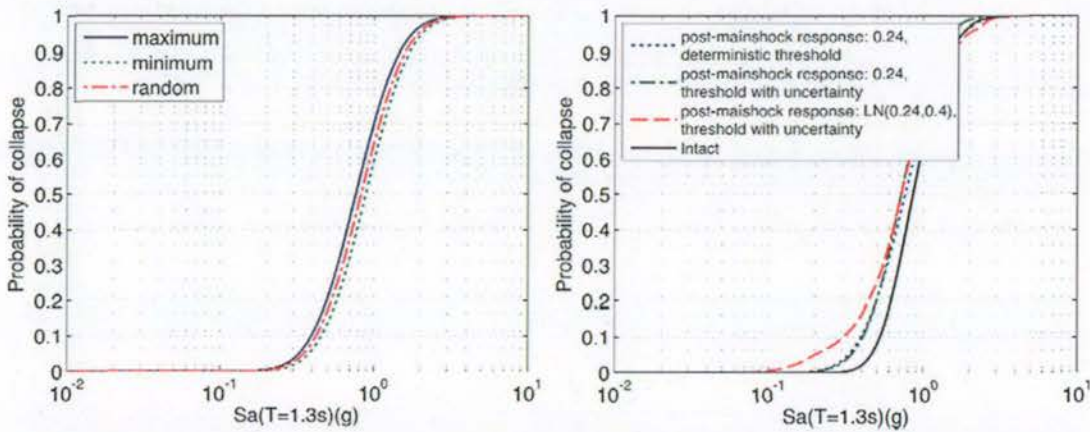


Figure 5 a) Comparison of three aftershock fragility curves depending on aftershock polarity; b) Comparison of three aftershock fragilities for a mainshock-damaged building against the collapse fragility for the undamaged (intact) building.

mainshock response corresponds to the extensive damage state, as also noted in Luco et al. (2004).

4 DISCUSSION

Figure 6a shows the median collapse capacity of the mainshock-damaged building versus mainshock response, using the deterministic mainshock response and deterministic threshold of collapse (see Equation 5). As alluded to in Section 3, the reduction in the median collapse capacity is small even for mainshock response beyond 0.29m, the median damage state threshold for complete damage. This surprising result is attributed to two observations. First, once the building experiences large nonlinear deformation, the characteristics of the damaged building, such as the fundamental period, change. Since the damaged model has a longer period, it might be less sensitive to the frequency content of an aftershock record than the undamaged or less-damaged building, as shown in Figure 6b. Second, the results depend on assumptions for cyclic deterioration and other nonlinear behavior. The cyclic deterioration model used in this study was not developed or verified for the simulation of nonlinear behavior of damaged buildings.

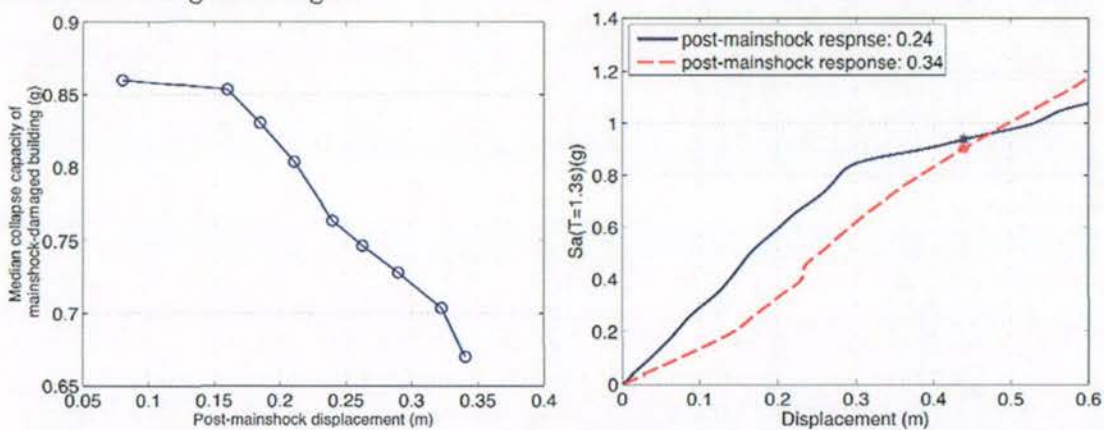


Figure 6 a) Median collapse capacity of mainshock-damaged building vs. mainshock response; b) Comparison of two aftershock IDA curves, whose post-mainshock responses are 0.24m and 0.34m, respectively.

Note that when we constructed IDA curves relating peak response to ground motion intensity, we only considered the building response due to the aftershock record, ignoring the peak mainshock response. As a result, the building has zero probability of collapse in low levels of aftershock ground motion intensity, as shown in Figure 5a and 5b. This was necessary for the purpose of computing damage

state transition probabilities, the probabilities of exceeding a higher damage state due to an aftershock, given a damage state caused by a mainshock. This should not be interpreted as ignoring mainshock damage in assessing post-aftershock damage states.

We also note that when selecting between two possible aftershock responses corresponding to the polarity of the aftershock record, it is more reasonable to select one randomly since it is unknown *a priori*; in other words, it is more reasonable to use the aftershock records as they are, which reduces the computational time by half.

5 SUMMARY

We present a methodology for developing fragilities for mainshock-damaged structures by performing incremental dynamic analysis (IDA) with a sequence of mainshock-aftershock ground motions. As an illustration of the methodology, we developed collapse fragilities for a typical New Zealand 5-storey reinforced concrete moment frame building, both undamaged and mainshock-damaged. Major conceptual improvements were made compared to the methodology in Luco et al (2004). Firstly, the proposed methodology is able to take into account uncertainty in the mainshock response for a given post-mainshock damage state. Second, the proposed methodology is able to take into account uncertainty in damage state thresholds when deriving the aftershock fragility.

The computed collapse fragility of a mainshock-damaged building can be coupled with the aftershock ground motion hazard at the location of the building in order to compute daily probability of collapse in an aftershock (Luco et al., 2011). This information helps structural engineers to assess whether a damaged building can continue to be occupied after a mainshock.

6 ACKNOWLEDGEMENTS

The work described in this paper has been carried out as a part of an EQC project (10/592) funded by the EQC Biennial Grants Programme 2010.

REFERENCES:

- Federal Emergency Management Agency (FEMA). 2003. HAZUS-MH MR-1 Technical Manual, Federal Emergency Management Agency, Washington, D.C., USA.
- Ibarra, L.F. 2003. Global collapse of frames structures under seismic excitations. Ph.D. Thesis, Department of Civil and Environmental Engineering, Stanford University, Stanford, California, USA.
- Luco, N., Bazzurro, P., Cornell, C.A. 2004. Dynamic versus static computation of the residual capacity of a mainshock-damaged building to withstand an aftershock. 13th World Conference on Earthquake Engineering, Vancouver, Canada. Paper no. 2405.
- Luco, N., Gerstenberger, M., Ryu, H., Uma, S.R., Liel, A.B., and Raghunandan, M. 2011. A methodology for probabilistic post-earthquake risk assessment that accounts for aftershocks, 9PCEE Paper No. 210.
- McKenna, F. and Fenves, G.L. 2000. An object-oriented software design for parallel structural analysis. Advanced Technology in Structural Engineering, Proceedings of Structures Congress 2000, ASCE.
- Ryu, H., Luco, N., Baker, J.W. and Karaca, E. 2008. Converting HAZUS capacity curves to seismic hazard compatible building fragility functions: effect of hysteretic models. The 14th World Conference on Earthquake Engineering, October 12-17, Beijing, China.
- Uma, S.R., Ryu, H., Luco, N., Liel, A.B., Raghunandan, M. 2011. Comparison of main-shock and aftershock fragility curves developed for New Zealand and US buildings, 9PCEE Paper No. 227.
- Vamvatsikos, D. and Cornell, C.A. 2006. Direct estimation of the seismic demand and capacity of oscillators with multi-linear static pushovers through IDA. Earthquake Engineering and Structural Dynamics, 35, pp.1097-1117.

This page is intentionally left blank.

APPENDIX 3: COMPARISON OF MAIN-SHOCK AND AFTERSHOCK FRAGILITY CURVES DEVELOPED FOR NEW ZEALAND AND US BUILDINGS



Proceedings of the Ninth Pacific Conference on Earthquake Engineering
 Building an Earthquake-Resilient Society
 14-16 April, 2011, Auckland, New Zealand

Comparison of main-shock and aftershock fragility curves developed for New Zealand and US buildings

S.R Uma

GNS Science, Avalon, Lower Hutt, New Zealand.

H. Ryu

University of Colorado at Boulder, Colorado, USA

N. Luco

US Geological Survey, Golden, Colorado, USA

A.B. Liel & M. Raghunandan

University of Colorado at Boulder, Colorado, USA.

ABSTRACT:

Seismic risk assessment involves the development of fragility functions to express the relationship between ground motion intensity and damage potential. In evaluating the risk associated with the building inventory in a region, it is essential to capture 'actual' characteristics of the buildings and group them so that 'generic building types' can be generated for further analysis of their damage potential. Variations in building characteristics across regions/countries largely influence the resulting fragility functions, such that building models are unsuitable to be adopted for risk assessment in any other region where a different set of building is present. In this paper, for a given building type (represented in terms of height and structural system), typical New Zealand and US building models are considered to illustrate the differences in structural model parameters and their effects on resulting fragility functions for a set of main-shocks and aftershocks. From this study, the general conclusion is that the methodology and assumptions used to derive basic capacity curve parameters have a considerable influence on fragility curves.

1 INTRODUCTION

Regional seismic risk assessment requires building fragility functions to be developed for building portfolios to represent probabilities of potential damage due to earthquake hazard. The regional building portfolio is divided into various building classes based on structural system, height and construction material. Further, a typical building is identified with certain parameters to represent that building class. Note that the generic characteristics of typical buildings vary across countries and, therefore, building fragility functions developed for one region may not be appropriate to be used in some other region where a different building portfolio is to be represented. For example, HAZUS (1999), a risk assessment tool, uses fragility functions specifically for the US building inventory. The parameters used for developing these fragility functions were mostly based on expert opinion and engineering judgement. To assess seismic risk in any other country with different building characteristics, the HAZUS based fragility functions may not be suitable. In New Zealand, 'Riskscape' a multi-hazard risk assessment tool (under joint development by GNS and NIWA), includes a building classification system similar to HAZUS, but for typical NZ buildings (King et al., 2009).

Risk assessment tools often consider risk due to a main-shock event only. However, it is not uncommon to get many aftershocks after the main-shock, some of which could be strong enough to cause further damage to the building. In such situations, it is necessary to estimate the residual capacity of main-shock damaged buildings. Luco et al., (2004) have addressed a methodology to determine the residual capacity of main-shock damaged buildings which could be adopted to develop 'aftershock fragilities'. A methodology to derive these aftershock fragility curves has been proposed by Ryu et al. (2011).

Considering the variability in building characteristics between regional building classes, an attempt has been made by the authors to illustrate the differences in fragility functions between US and NZ building models. In this regard, a typical five storey building representing medium-rise reinforced concrete moment resisting frames has been chosen to be modelled to represent US and NZ building stock, respectively.

Non-linear incremental dynamic analyses are carried out on both US and NZ models for a suite of main-shock and aftershock records. Five different damage states are defined, slight, moderate, extensive, complete and collapse, and associated fragility functions developed. Damage state thresholds are defined based on criteria established in previous work (Ryu, 2008). Fragility functions are derived for US and NZ models for a main-shock and possible aftershocks event of magnitude (M) within a specified range.

2 GENERIC BUILDING MODELS FOR REGIONAL RISK ASSESSMENT

One of the biggest challenges in deriving a fragility/vulnerability model is to acquire an appropriate building inventory database. In developing building classification systems for Riskscape, pilot studies were conducted on three regions (Christchurch, Hawke's Bay and Westport) to represent the building types common within New Zealand. The three regions were chosen as representatives of distinctly different categories, viz. large city (about 300,000 buildings), small city/rural (30,000 buildings) and town (2000 buildings). Generic buildings are defined based on the building characteristics, including height and structural system adopted to resist lateral loads. HAZUS has included a total of 36 generic building models for the US building inventory. In Riskscape, 18 building classes have been identified for the NZ building inventory and generic characteristics of building classes are listed elsewhere (King et al, 2009). It is worth mentioning that while developing building classifications for Riskscape, it was kept in mind to follow similar grouping systems with respect to number of storeys as in HAZUS; i.e. (a) low-rise buildings (up to 3 storeys); (b) medium-rise buildings (4-7 storeys); and (c) high-rise (8 storeys or more) in the interest of seeking some common basis.

It is to be noted that the fragility functions for 'generic buildings' are developed based on the response of a typical building with generic structural properties and hence cannot be directly applicable for building-specific risk assessment purposes. The structural models for a generic building within a building class should preferably be determined after accounting for the variability in building characteristics of that building class.

2.1 Parameters for capacity curves

Estimation of building response requires developing representative building models either in the form of single-degree-of-freedom (SDOF) models or multi-degree-of-freedom (MDOF) models. Unlike a MDOF model where building details are explicitly specified, a SDOF model is defined using a capacity curve with a certain number of control points. For example, the HAZUS methodology proposed curvilinear capacity curves as shown in Figure 1 (a) using two sets of control points at yield (A_y, D_y) and ultimate (A_u, D_u) capacities. The HAZUS capacity curve remains plastic, without any strength degradation after reaching ultimate capacity, which is unrealistic. Also, the ratio of ultimate to yield displacement, (i.e., the effective ductility), is too large for real structures. This is because the ultimate displacement capacity is not the 'true' ultimate displacement capacity of the system. It is just a point along the capacity curve at which the maximum strength has been fully attained. SDOF models based on these parameters are appropriate for use in the capacity spectrum method, and not where

non-linear time history analyses are involved.

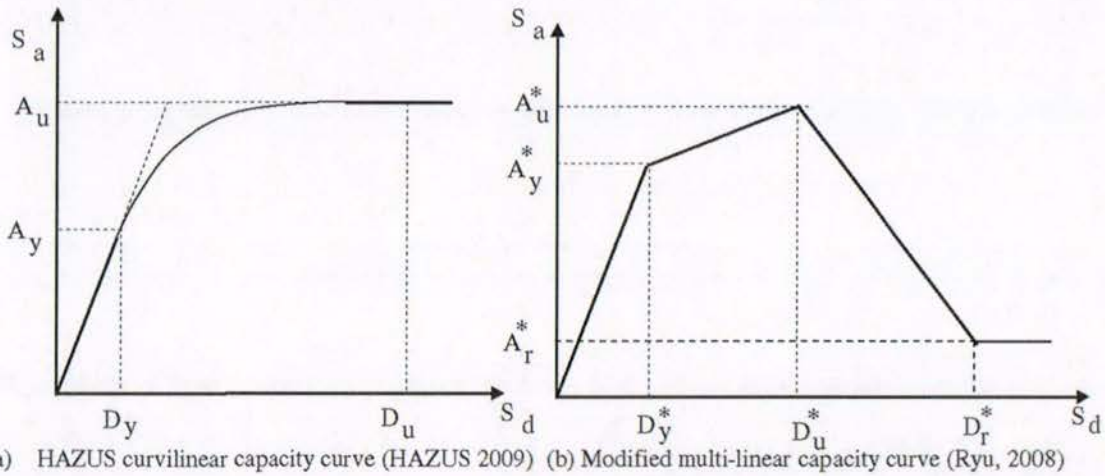


Figure 1 Capacity curve definitions for single-degree-of-freedom (SDOF) model

As an alternative to the HAZUS curvilinear curve, Ryu et al (2008) proposed a multi-linear capacity curve with a negative stiffness after the ultimate (capping) point to include degradation in system performance. The proposed multi-linear capacity curve has yield (A_y^* , D_y^*), ultimate (A_u^* , D_u^*) and residual (A_r^* , D_r^*) capacity points, which are more suitable to describe non-linear dynamic SDOF models.

In this study, building models for a five storey reinforced concrete moment-resisting frame are idealised as SDOF models and defined with multi-linear capacity curves. The basic parameters necessary to define the model are the displacement and base shear coefficient at the yield point (A_y^* , D_y^*) where 'significant yield' is expected; the ultimate displacement, defined by structural ductility; and the ultimate capacity, defined in terms of the strain-hardening ratio with respect to yield capacity. The residual strength is assumed as 20% of yield strength. The residual displacement (D_r^*) is considered to be coinciding with 'collapse' damage state thresholds and the values are given in Table 2.

The bases for selecting parametric values on the multi-linear curves for NZ and US models are discussed below.

2.2 NZ building model

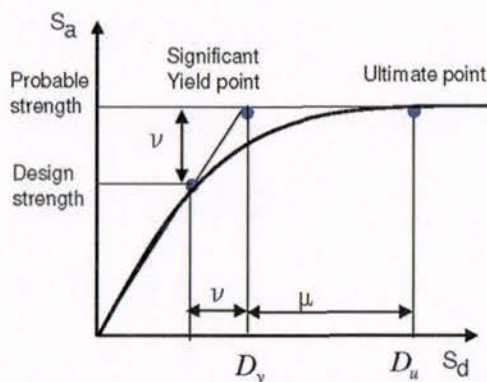


Figure 2. Idealised capacity curve (Ref: Park, 1997)

A typical five storey reinforced concrete frame with a total height of 18m is considered for this study. The proposed capacity curve is given in Figure 2 (Park, 1997). The 'design strength' refers to the code-specified lateral strength where the first plastic hinge is assumed to be forming. Further plastic hinges form to reach the 'significant yield point' where a mechanism forms. The probable strength is obtained using a factor, ν , to account for the probable overstrength of the material (taken as 1.25) and the redundancies (taken as 1.75) in the structural system. The 'ultimate point' is ductility ' μ ' times the yield displacement. Based on a displacement based approach (Priestley et al., 2007), the yield

displacement is determined. This approach uses mechanically-derived formula (or equations) to describe yield displacement capacity using geometrical and material properties. A Monte-Carlo procedure is adopted to simulate the geometrical and material property variables for the typical building. The structural characteristics of the NZ building model are assumed to be within the range of values assigned for medium-rise buildings as shown in Table 1. Note that U[] represents uniform distribution and N[] represents normal distribution for the variables. Further details on the range of variables considered for simulation for a medium-rise reinforced concrete moment-resisting frame are presented elsewhere (Uma et al, 2010). From simulation, the median displacement is chosen as the yield displacement for the model. A limited ductility of 3 is considered so that ultimate point is close to a 2% drift ratio; the ultimate strength at ultimate point is obtained with a low post-yield stiffness ratio of 5%.

The initial period is computed based on the recommendations in the Commentary to NZS1170.5:2004 (SNZ, 2004). The building periods, based on code recommendations, are usually conservative for estimating design base shear, and less than the 'true' value. The median initial period is estimated on the higher side, considering a reasonable amount of variation from the initial period recommended for design purposes. The initial period for the NZ model is taken as 1.3s. The design strength is obtained from NZ 1170.5:2004 design spectra for site subsoil class 'C' and for the Wellington region with a hazard coefficient of $Z=0.4$, and the probable strength is obtained after accounting for overstrength factors as mentioned above.

Table 1. Structural parameters for concrete moment-resisting frame structures.

Structural Parameters	Range of values	Structural Parameters	Range of values
Number of storeys, N_s	U [4,7]	Beam depth (m), h_b	U [0.5, 0.7]
Storey height (m), S_h	U [3.4, 3.8]	Steel strength (MPa), f_y	N [325,35]
Beam length (m), l_b	U [5.0, 7.0]	Effective height coeff., efh	$0.64-0.0125*(N_s-4)$

2.3 US building model

A comparable HAZUS building type CIM with a HAZUS-suggested ductility of 5.3 is chosen to represent a typical five storey building with a height of 50 feet (about 15.24 m). The original HAZUS-based capacity curve parameters are notably unrealistic. In this regard, Ryu et al., (2008) suggested a modified procedure to construct a multi-linear capacity curve where the yield and ultimate capacity points are determined via an iterative procedure.

Table 2. Parameters to define multi-linear capacity curves for NZ and US models.

	Ty, s	Yield		Ultimate		Residual	
		D _y , m	A _y [*] , g	D _u , m	A _u [*] , g	D _r , m	A _r [*] , g
NZ model	1.3	0.08	0.20	0.24	0.22	0.44	0.044
US model	0.75	0.06	0.46	0.34	0.62	0.61	0.09

The building period is taken as 0.75s as suggested by HAZUS. The original yield strength, A_y , accounts for overstrength and is about 0.2g which is very close to the probable strength of the NZ model. The iterative procedure is based on 'equal area principle' within the curvilinear portion and assumes the initial stiffness suggested by HAZUS which is unaltered for determining the 'significant yield' point (Ryu, e al., 2008). The yield base shear coefficient A_y obtained from the above iterative procedure resulted in a much higher value than that for the NZ building. The ultimate displacement point is ductility times the significant yield point. The ultimate capacity is taken with an 8.5% strain-hardening ratio from yield capacity, and the residual capacity is 20% of the ultimate capacity. Figure 3

shows the plots of multi-linear capacity curves for NZ and US building models and Table 2 lists the values.

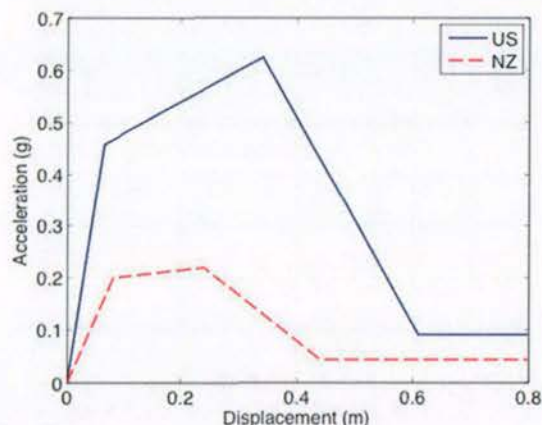


Figure 3. Multi-linear capacity curves for NZ and US models

fundamental period because 1) the system will have a longer period if it becomes inelastic or nonlinear; 2) in incremental dynamic analyses (IDA) curves, responses from longer periods show less variability.

4 FRAGILITY CURVES

Fragility curves are expressed as cumulative lognormal distribution curves and are developed for five damage states. The median damage state threshold values in terms of roof displacement are given in Table 3 for the NZ and US building models.

Table 3. Damage state thresholds considered for NZ and US models

Damage state	Description	NZ model (m)	US model (m)
1	slight	0.08 (0.7%)	0.06 (0.5%)
2	moderate	0.16 (0.14%)	0.16 (0.14%)
3	extensive	0.24 (2.0%)	0.34 (3.0%)
4	complete	0.29 (2.6%)	0.40 (3.5%)
5	collapse	0.44 (3.9%)	0.61 (5.3%)

The methodology to derive fragility curves considering the uncertainty in damage state thresholds is discussed in a companion paper (Hyeuk, 2011). A lognormal standard deviation of 0.4 is considered to represent the uncertainty in damage state thresholds.

4.1 Fragility curves for mainshocks

Incremental dynamic analyses are performed on SDOF non-linear models described by multi-linear capacity curves with parameters as shown in Figure 2. The time history analyses adopt a pinching hysteretic model to simulate strength and stiffness degradation within the system. The procedure to develop fragility curves from incremental dynamic analyses is described in detail in Ryu et al. (2011). The fragility curves derived for US and NZ models are shown in Figure 4. It is clear that the median $Sa(T=1.3s)$ values for the US models are higher than that those for the NZ models. The reason is that the US model is characterised by higher capacity and is associated with damage state threshold points

3 GROUND MOTIONS

The suite of thirty records compiled by Vamvatsikos and Cornell (2006) is used for both main-shock and aftershock records. The moment magnitude of the records is within 6.5-6.9, and the closest distance to fault rupture of the records is within 15-33km. The fundamental period of the US model is 0.75sec and that for the NZ model is 1.3 s. Spectral acceleration at 1.3 s with a damping ratio of 5% is chosen as the ground motion intensity measure for both of the models. Selection of the $Sa(T=1.3s)$ intensity measure is mainly for comparison of the fragility curves generated by the models; it is justified to choose a longer period than the

at larger drift ratios.

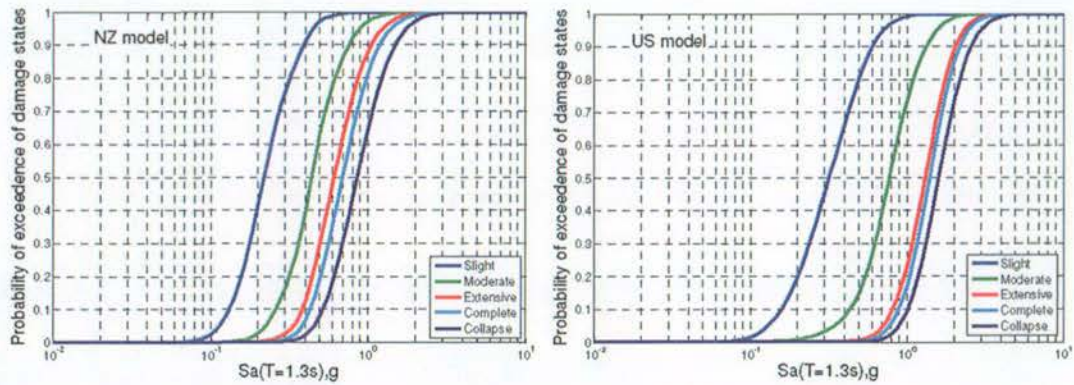


Figure 4. Fragility curves for all damage states due to main-shock records on NZ and US models

In order to compare the fragility curves from NZ and US building models, a common basis is established by setting the damage threshold points for the US model the same as those for the NZ model. A set of comparison plots for four damage states for the 'modified' US model and NZ model is shown in Figure 5.

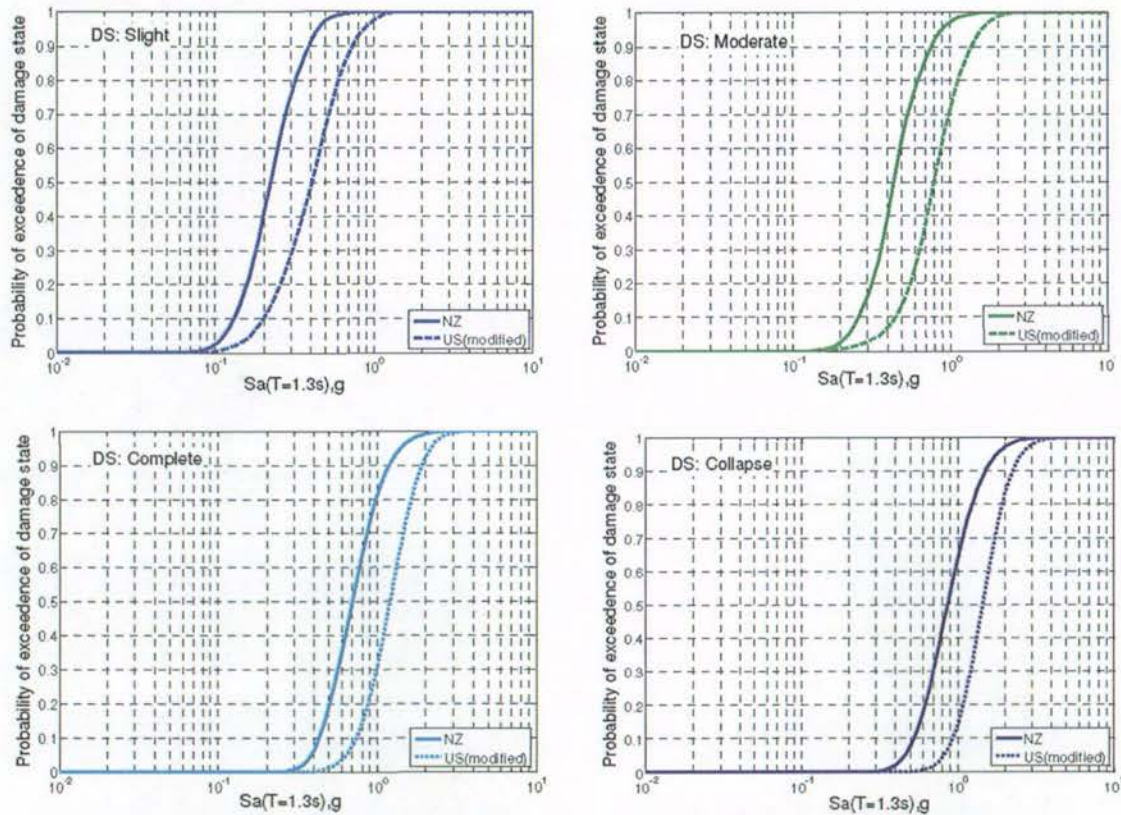


Figure 5 Comparison of fragility curves for the NZ and US models for damage states: Slight, Moderate, Complete and Collapse

Table 4. Median values of $S_a(T=1.3s)$ g and damage threshold drift ratios for various damage states

	Slight		Moderate		Extensive		Complete		Collapse	
	S_a ,g	Dr(%)	S_a ,g	Dr(%)	S_a ,g	Dr(%)	S_a ,g	Dr(%)	S_a ,g	Dr(%)
NZ	0.22	0.7	0.44	1.4	0.61	2.0	0.70	2.6	0.87	3.9
US(modified)	0.41	0.7	0.80	1.4	1.12	2.0	1.20	2.6	1.45	3.9
US	0.32	0.5	0.78	1.4	1.32	3.0	1.39	3.5	1.58	5.3

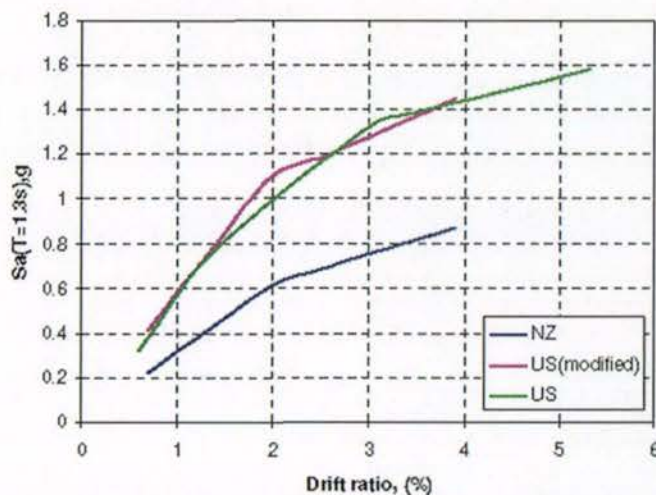
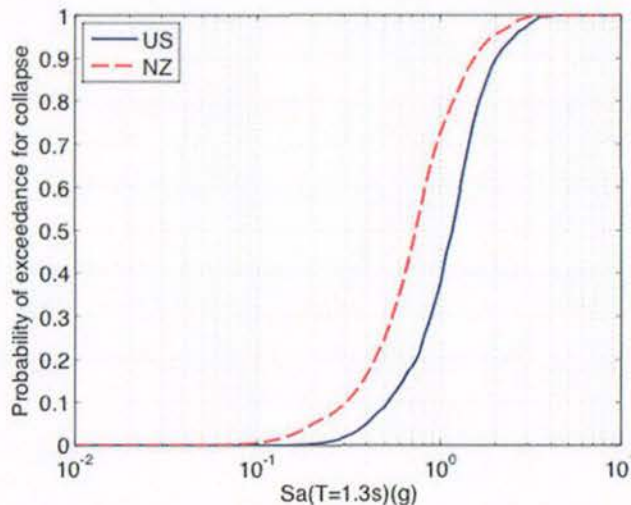
Figure 6 Variation of $S_a(T=1.3s)$,g with respect to drift ratio for NZ model and US models with different sets of damage threshold

Figure 7. Aftershock fragility curves for NZ and US models

a realization of main-shock damage due to a particular main-shock), 30 aftershocks are applied to estimate seismic demands on main-shock-damaged building. The procedure to compute fragility for aftershocks is described in detail in Ryu et al. (2011). Figure 7 compares the collapse fragilities when the models are in an 'Extensive' damage state due to the main-shock. It is clear that the residual

From the fragility curves shown in Figures 4 and 5, only the median S_a values at all damage states are plotted against drift ratios in Figure 6. It is evident that S_a values are influenced by the stiffness and strength of the building models. The S_a values of the US models are about 1.9 times those for the NZ model up to the 'Extensive' damage state and about 1.7 times those for NZ model for 'Complete' and 'Collapse' damage states. Overall, it is apparent that the fragility functions are highly sensitive to the maximum capacity of the building model.

4.2 Fragility curves for aftershocks

In addition to comparison of main-shock fragilities between US and NZ models, we compared fragilities for buildings damaged under the main-shock. For this illustration, post-main-shock damage is assumed to be in the extensive damage state, and the post-main-shock response is assumed to follow a lognormal distribution, with a median damage state threshold for the 'Extensive' damage state of 0.24 and 0.34 for the US and NZ models respectively. For each realisation of the main-shock-damaged model, which was simulated by subjecting the model to a main-shock record to get it to have the predefined post-main-shock response, we perform incremental dynamic analyses using the aftershock records. For each main-shock record (specifically, a

capacities of the buildings having 'Extensive' damage from 'Collapse' (1.16g and 0.73g for US and NZ buildings respectively: Figure 7) are less than those for intact (undamaged) buildings to from reaching the Collapse damage state (1.59g and 0.86g for US and NZ buildings respectively: Figure 4).

5 SUMMARY

In this study, fragility functions developed for five storey buildings typically representing medium-rise reinforced concrete frames in US and NZ are presented. The dynamic responses of the buildings are determined by incremental dynamic analyses of SDOF models. The differences in fragility functions between the US and NZ models arise because of the assumptions involved in developing the capacity curve parameters for the SDOF models. Some level of engineering judgement and empirical expressions are used to arrive at the control parameters. The variability in building characteristics to represent a building class is considered through simulation. In general, modified HAZUS parameters for both drift and strength that define the US model are higher than the parameters evaluated for the NZ model.

Since the fragility functions are influenced by the basic capacity curve parameters and the procedure involves considerable computational effort in carrying out incremental dynamic analyses (IDA), it is an imperative that the parameters for SDOF models are predicted with better approaches (e.g. by pushover analyses on MDOF models) and not only based on engineering judgement. Currently, work is ongoing in developing fragility curves for older reinforced concrete frames modelled as two dimensional frames with non-ductile beam, column and joint elements.

From the present study, it appears that the NZ models are more fragile than US models, both with regard to main-shocks and aftershocks, but this observation is not conclusive without carrying out detailed studies with better structural models representing 'true' characteristics to predict their non-linear dynamic responses.

6 ACKNOWLEDGEMENTS

The work is being carried out as a part of EQC project (10/592) funded by EQC Biennial Grants Programme 2010. The authors thank Dr Matt Gerstenberger and Dr Jim Cousins for their review comments.

7 REFERENCES:

- HAZUS .1999. Earthquake loss estimation methodology. Prepared by: Risk Management Solutions, Funded by FEMA, Washington D.C.
- King, A.B. and Bell, R. 2009. Riskscape Project 2004-2008. GNS Science consultancy report 2009.247, October 2009. 162p.
- Luco, N., Bazzurro, P., Cornell, C.A. 2004. Dynamic versus static computation of the residual capacity of a mainshock-damaged building to withstand an aftershock. 13th World Conference on Earthquake Engineering, Vancouver, Canada. Paper no. 2405.
- SNZ 2004. NZS1170.5. Structural Design Actions Part 5 Earthquake actions - New Zealand, Commentary, Standards New Zealand, Wellington, New Zealand.
- Park, R. 1997. A static force-based procedure for the seismic assessment of existing reinforced concrete moment resisting frames. Bulletin of the New Zealand Society of Earthquake Engineering 30(3):213-226.
- Priestley, M.J.N., Calvi, G.M., 2007. Displacement-based seismic design of structures. IUSS Press, Pavia, Italy.
- Ryu, H., Luco, N., Baker, J.W. and Karaca, E. 2008. Converting HAZUS capacity curves to seismic hazard compatible building fragility functions: effect of hysteretic models. The 14th World Conference on Earthquake Engineering, October 12-17, Beijing, China.
- Ryu, H., A.B. Liel, N. Luco and S.R. Uma 2011 Developing fragilities for mainshock-damaged structures through incremental dynamic analysis, 9PCEE Paper No. 225.

- Uma S.R. and Bradley, B. 2010 b. Displacement based fragility functions for New Zealand buildings subject to ground motion hazard. Proceedings, Asian Conference on Earthquake Engineering, December 1-3, Bangkok, paper No. 72.
- Vamvatsikos, D. and Cornell, C.A. 2006. Direct estimation of the seismic demand and capacity of oscillators with multi-linear static pushovers through IDA. Earthquake Engineering and Structural Dynamics, 35, pp.1097-1117.

**APPENDIX 4: AFTERSHOCK FRAGILITY CURVES AND TAGGING
ASSESSMENTS FOR A MAINSHOCK-DAMAGED BUILDING**

Aftershock Fragility Curves and Tagging Assessments for a Mainshock-Damaged Building

M. Raghunandan & A.B. Liel

University of Colorado at Boulder, Boulder, CO USA

H. Ryu

Geoscience Australia, Canberra, ACT Australia

N. Luco

US Geological Survey, Golden, CO USA

S.R. Uma

GNS Science, Avalon, Lower Hutt, New Zealand



15 WCEE
LISBOA 2012

SUMMARY:

When multiple earthquakes occur within a short period of time, damage may accumulate in a building, affecting its ability to withstand future ground shaking. This study aims to quantify the post-earthquake capacity of a non-ductile 4-story concrete building in New Zealand through incremental dynamic analysis of a nonlinear multiple-degree-of-freedom simulation model. Analysis results are used to compute fragility curves for the intact and damaged buildings, showing that extensive damage reduces the structure's capacity to resist seismic collapse by almost 30% percent. The damage experienced by the building in mainshock, can be compared with the ATC-20 building tagging criteria for post-earthquake inspections, the purpose of which is to ensure public safety. Extensively damaged buildings, which are likely to be *red* tagged, pose a significant safety hazard due to decreased strength in future earthquakes. The effect of mainshock damage is also compared for multiple and simplified single-degree-of-freedom models of the same building.

Keywords: Aftershocks, Non-ductile concrete buildings, Collapse, Post-earthquake safety

1. INTRODUCTION

Buildings in seismically active regions may be at the risk of experiencing multiple earthquakes or mainshock-aftershock sequences in quick succession. Structures in Christchurch, New Zealand experienced such a sequence of earthquakes, when, first, a M_w 7.0 event in September, 2010, and, subsequently, a M_w 6.1 event in February, 2011, caused extensive damage to the built environment, much of which is still awaiting repair (Smyrou et al., 2011). The March, 2011 M_w 9.0 Tohoku, Japan earthquake was followed by hundreds of aftershocks as large as M_w 7.9, including at least 30 aftershocks greater than M_w 6.0 (USGS, 2011). Due to the close timing of these types of events, repair or retrofit activities are often not possible before the next earthquake, increasing the risk of further damage or collapse of already damaged buildings. The quantification of damage in buildings in earthquake sequences can equip us with the tools to mitigate the damage to the life and property as a result of better understanding of the building response and the building fragility in these events. Findings have important implications for post-earthquake inspections and building tagging procedures, which are intended to provide public safety after an earthquake.

There is significant ongoing research to understand the influence of mainshock-aftershock sequences and repeated earthquakes on steel and concrete buildings. A few of the studies have used nonlinear multiple-degree-of-freedom (MDOF) models to examine the response of steel structures (Fragiacomo et al., 2004; Lee and Foutch, 2004; Li and Ellingwood, 2007; Ruiz-García and Negrete-Manriquez, 2011), concrete bridges (Ruiz-García et al., 2008) and concrete frames (Hatzigeorgiou and Liolios, 2010) under earthquake sequences, while most other studies employed single-degree-of-freedom (SDOF) models (Sunasaka and Kiremidjian, 1993; Amadio et al., 2003; Hatzigeorgiou and Beskos,

Peer Review DISCLAIMER: This draft manuscript is distributed solely for purposes of scientific peer review. Its content is deliberative and predecisional, so it must not be disclosed or released by reviewers. Because the manuscript has not yet been approved for publication by the U.S. Geological Survey (USGS), it does not represent any official USGS finding or policy.

2009; Hatzigeorgiou, 2010) for understanding structural behavior under earthquake sequences. Luco et al. (2004) proposed a probabilistic methodology to compute the residual capacity of mainshock-damaged buildings in terms of the ground motion intensity of an aftershock that can cause collapse or some other damage state. Using this methodology, Ryu et al. (2011) developed equations for building fragility in mainshock and aftershocks, implementing the procedure for SDOF analysis.

This study computes mainshock and aftershock building fragility curves of non-ductile concrete frame-type buildings, and relates the damage predicted to the building tagging criteria provided in documents available to assess the post-earthquake building safety, such as ATC-20 (ATC, 1989, 1995) and the New Zealand Society for Earthquake Engineering Building Safety Evaluation Guidelines. In ATC-20, rapid visual evaluations assign a building into three categories: 1) *green* tag or INSPECTED and safe to use, 2) *yellow* tag or RESTRICTED USE, *i.e.* requiring further detailed evaluation, or 3) *red* tag declaring building to be UNSAFE to occupy. These inspections take around 10-20 minutes per building, requiring a lot of time to inspect and tag all of the buildings in a region. The guidelines to describe the damage states are also qualitative and tagging decisions can vary depending on inspection personnel. For example, in ATC-20, a reinforced concrete frame building is to be tagged *red* if there is a collapse or partial collapse, or noticeable leaning in a building or individual story, or failure or incipient failure of columns, or serious degradation in column or beam elements, or severe panel zone cracking (ATC, 1989, ATC, 1995). The *red* tagging will be based on how severe the building inspector finds the building's condition. Probabilistic prediction of the probable damage during an aftershock on a typical building damaged during a mainshock, together with site-specific aftershock hazard information, will help in prioritizing regions for post-earthquake inspection. A more quantitative tagging criterion can provide clearer guidelines, eliminating a lot of *yellow* tagging in the process.

This paper describes the probabilistic methodology utilized to study the influence of the earthquake sequences on building capacity in the performance-based earthquake engineering framework. This probabilistic methodology utilizes nonlinear simulations of archetypical building models to assess the probable damage to the buildings subjected to multiple earthquakes. In this study, incremental dynamic analysis is carried out on the nonlinear MDOF analytical model of a typical non-ductile 4 story building in New Zealand, which is typical of structures built there in the 1960's or early 1970s. The building model is capable of capturing the critical aspects of strength and stiffness degradation of the building as the damage progresses, potentially leading to collapse. Nonlinear static pushover and dynamic analyses on the intact building are used to quantify the damage states thresholds, *i.e.* the displacement-based limits at which a particular damage state occurs. To quantify aftershock damage, the building is then subjected to a large number of earthquake sequences, such that the mainshock in the sequence brings the building into a particular damage state and the aftershock affects the damaged building. The damage observed in the intact buildings due to earthquake sequences can be linked back to the ATC-20 criteria for post-earthquake safety evaluation. Since the analysis of MDOF models subjected is computationally intensive, a similar analysis on a SDOF model calibrated to the same New Zealand building is conducted and results are compared.

2. BUILDING MODEL

Nonlinear dynamic analysis of mainshock-aftershock sequences is carried out on the numerical model of a typical 1960s era non-ductile 4-story New Zealand building. The non-ductile building model geometry, along with beam and column section and reinforcement properties, is shown in Fig. 2.1(a). These frames are potentially susceptible to brittle flexure-shear or shear-critical failure modes, due to low quantity and detailing of transverse reinforcement (typically spaced at 14 inches). The building has a flooring system prevalent in older New Zealand construction consisting of prestressed concrete ribs with permanent timber formwork and an in-situ concrete topping, supported by the building's primary beams. This floor system does not affect the strength of the beams (*i.e.* no slab effect). This flooring system results in significantly lower dead loads compared to a flat slab floor.

The analytical building model is implemented in *OpenSees* (2011), an open-source, object-oriented structural analysis platform developed by the Pacific Earthquake Engineering Research Center. The

3.1, and illustrated in Fig. 3.1(b). Table 3.1 also reports the maximum roof drift and residual interstory drifts observed at the onset of each of the various damage states during the pushover analysis. The damage state thresholds in terms of roof drifts are used to calibrate the SDOF model.

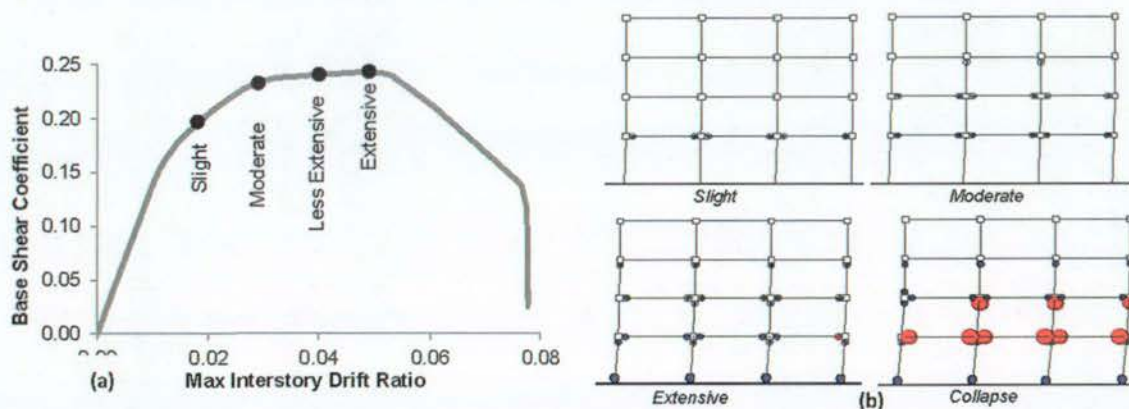


Figure 3.1 (a) Pushover analysis results for the building, showing the drift level thresholds associated with each damage state; (b) The physical state of building during each of the defined damage states.

This analysis assumes deterministic damage states, such that it is assumed that physical damage will occur during the dynamic analysis at the drift threshold defined for each damage state. In reality and as seen in dynamic analysis, depending on the characteristics of the ground motions, the physical damage states may not occur at the same interstory drift ratios as in the pushover analysis. Fig. 3.2(a) illustrates this variation in the drift levels at damage state initiation, where the labeled “individual IDA” correspond to the drift levels at which the physical states of slight, moderate, and extensive damage was observed during incremental dynamic analysis for each of 30 ground motions (Section 4.2). The drift thresholds identified in pushover analysis are very close to the median observed in dynamic analysis results. Similar relationships between median maximum roof drift from dynamic analysis and pushover analysis is also observed. Residual drifts are not used to define damage states, but are reported here because they may strongly influence structural behavior during the aftershock (Luco et al., 2004).

Table 3.1 Damage state descriptions, along with the damage state thresholds defined for the building.

Damage State	Physical Description	Max Interstory Drift	Roof Drift
Slight	Yielding of all beam hinges at one floor	0.018	0.009
Moderate	Start of yielding of columns	0.029	0.014
Less Extensive	Intermediate damage state ¹	0.040	0.020
Extensive	Plastic hinge rotation demand exceeding plastic hinge rotation capacity for at least one hinge in joint, beam or column	0.049	0.025
Collapse	Dynamic instability	0.12	0.060

¹“Less Extensive” does not correspond to a specific physical state, but shows an intermediate state between Moderate and Extensive.

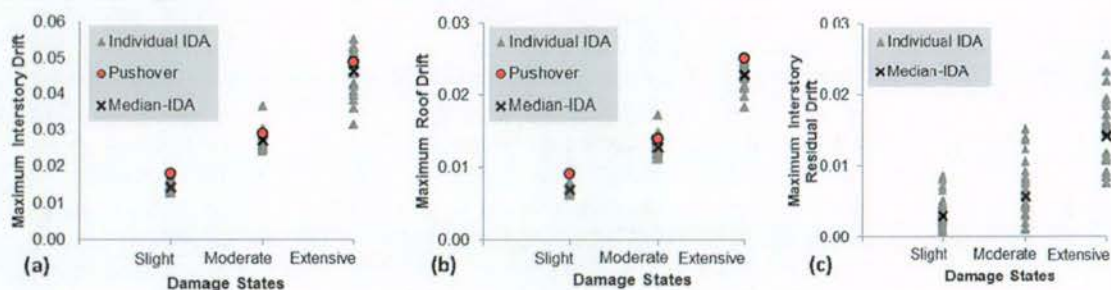


Figure 3.2 (a) Maximum interstory drifts, (b) roof drifts and (c) maximum residual interstory drifts associated with each damage state, as obtained from pushover and dynamic analysis.

4. NONLINEAR DYNAMIC ANALYSIS

4.1. Ground Motions

A set of 30 ground motions are used as both mainshock and aftershock records (Vamvatsikos and Cornell, 2006). These records are from California earthquakes with M_w between 6.5 and 6.9 and sites with closest distance to fault rupture within 15 to 33 km. Ground motions are recorded on firm soil with no directivity effects. The unscaled records have peak ground accelerations from 0.04 to 0.63g.

The ground motion intensity is measured using inelastic spectral displacement at the fundamental period of the structure, denoted S_{di} (Tothong and Cornell, 2006). Inelastic spectral displacement is defined as the peak displacement that a SDOF bilinear oscillator experiences when subjected to the ground motion. For this computation, the oscillator is assumed to have a 5% damping, and a pre-defined yield displacement (5.106 inches), which can be computed from the nonlinear pushover results (FEMA, 2009). The post-yield hardening stiffness for the oscillator is taken as 5% of initial stiffness. Research by Baker and Cornell (2006) has shown that structural response is significantly affected by ground motion spectral shape as well as spectral intensity. The conventionally-used intensity measure, elastic spectral acceleration, represents only spectral values at the fundamental building period. In fact, the spectral acceleration or displacement at many other periods becomes important for a building experiencing severely nonlinear behavior because its period elongates as damage occurs and the higher modes influence the response. S_{di} accounts for the longer natural periods as the bilinear oscillator yields and undergoes period elongation, thereby providing a simple measure for incorporating important spectral shape effects in addition to ground motion intensity.

4.2. Incremental Dynamic Analysis Procedure

To quantify the response of the building in the event of an earthquake or a sequence of earthquakes, incremental dynamic analysis (IDA) is carried out on the nonlinear building model *OpenSeesMP* (parallel version of *OpenSees*). In IDA, the nonlinear building model is subjected to a ground motion having a particular intensity (calculated here in terms of intensity measure S_{di}), and its response is recorded, including demand parameters such as maximum interstory drifts, maximum residual drifts or roof drifts (Vamvatsikos and Cornell, 2002). In subsequent analyses, the ground motion is scaled to a larger intensity and the nonlinear dynamic response again recorded. The process of repeated scaling of ground motions and dynamic analysis is continued until the structure collapses, which is indicated by dynamic stability (*i.e.*, very large interstory drifts, or roof drifts in case of SDOF). The incremental dynamic analysis process provides insights about structural behavior under rare, high-intensity ground shaking, for which few recordings are available. To account for the effect of record-to-record variability on structural response, IDA is repeated for each of the 30 ground motions in the set.

As the first step in the analysis, IDA is carried out on the nonlinear model of the intact New Zealand building, as illustrated in Fig 4.1(a); the bold (red) line highlights IDA results from one (of 30) ground motions. These results quantify the ground motion intensity the structure can withstand before experiencing a particular damage state. Due to differences in frequency content, duration and other ground motion characteristics, each ground motion is scaled to a different intensity before a particular damage level occurs; for example, depending on the ground motion, the building of interest reaches the moderate damage state (0.029 interstory drift) at S_{di} levels between about 5 and 9 inches (Fig. 4.1(a)). A fragility curve summarizes IDA results for each damage state, showing the probability of being in (or exceeding) a particular damage state as a function of ground motion intensity, as shown in Fig. 4.1(b). These fragility curves are computed based on the interstory drift damage state thresholds (Ryu et al. 2011). For example, Fig. 4.1(b) shows that the median S_{di} intensity necessary to cause at least moderate damage in the building is 7.62 inches. The standard deviation in the fragility represents differences in frequency content and other ground motion characteristics. For comparison purposes, Fig. 4.1(b) also shows fragility curves for the intact building obtained from the SDOF model. In most

cases the median capacities associated with each damage state are similar for the two models (1-11% different). However, the single-degree-of-freedom predicts smaller standard deviations, indicating that record-to-record variation is less significant for the simpler model.

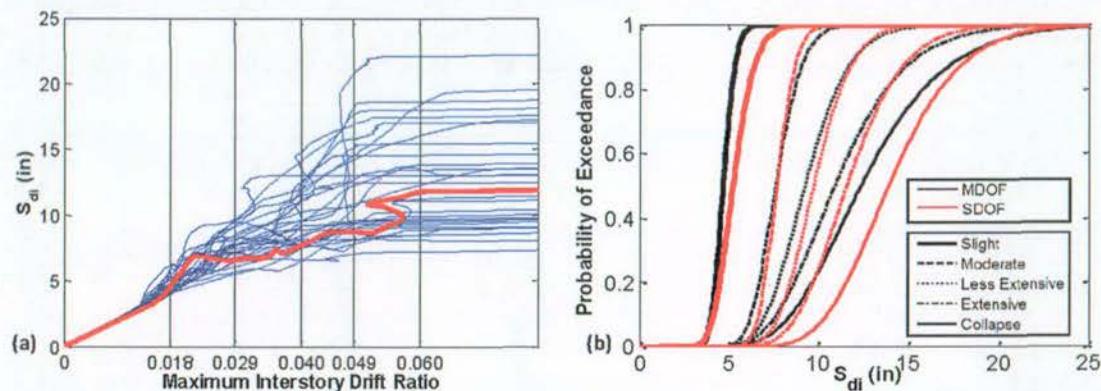


Figure 4.1 (a) IDA results (Note: the interstory drift values shown on the x-axis in Fig. 4.1 (a) correspond to the discrete damage states defined earlier); (b) Fragility curves for the intact New Zealand Building (black). The fragility curves for the intact SDOF model (red) are shown for comparison.

The aftershock analysis subjects the building to a mainshock-aftershock sequence, as shown in Fig. 4.2. The mainshock record is scaled to achieve a particular damage state in the structure and, subsequently, an aftershock record applied to the mainshock-damaged structure. A total of 900 earthquake sequences are created by combining each of the 30 mainshock ground motions with the same 30 ground motions applied as aftershocks. A rest period of four seconds is added between multiple earthquake events to recreate the real world situation, in which the structure comes to rest, but is not repaired. Dynamic analysis of the sequence is repeated with increasing scale factors applied to the aftershock record until the structure collapses, providing incremental dynamic analysis results for aftershocks. The aftershock response so obtained can be used to generate fragility curves for each damage state, but now conditioned on the damage experienced in the mainshock.

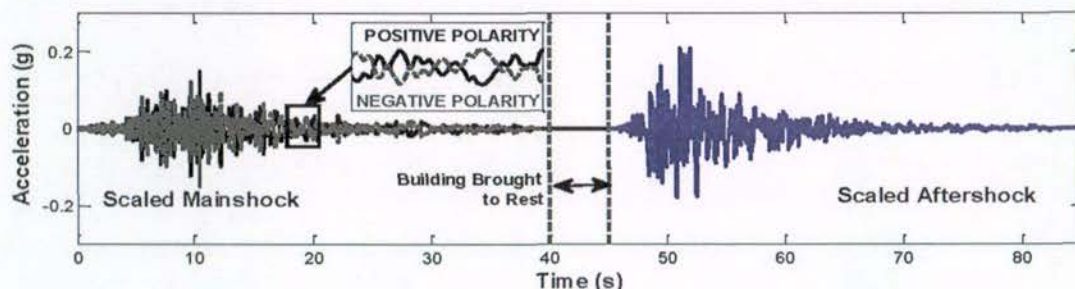


Figure 4.2 A mainshock-aftershock sequence for analysis of damaged building.

The issue of polarity of aftershock with respect to mainshock becomes important for cases where the residual drift after a mainshock is high (*i.e.* the structure is leaning to one side or another). The term “polarity” refers to the directions of the aftershock and mainshock, and specifically whether the aftershock is applied in the same direction or in the opposite direction as mainshock, tending to increase or reduce residual drift. To quantify the influence of polarity, polarities of the mainshock records were reversed in the analysis of both moderate and extensively damaged buildings.

5. RESULTS

The results obtained from incremental dynamic analysis of the mainshock-aftershock sequence are shown in Fig 5.1, where the x -axis represents the maximum interstory drift ratio experienced by the

structure during the aftershock (second ground motion in sequence). Results are shown for both (a,c) a building moderately damaged in the mainshock and (b,d) a building extensively damaged in the mainshock. The thick black line indicates the incremental dynamic analysis results from a particular mainshock-aftershock sequence. In the region shaded in grey, the interstory drifts undergone during the aftershock are smaller than those experienced in the mainshock and are not considered while calculating the damaged-building fragility because the damage state is unchanged from the mainshock. There is significant scatter in the intensity levels at which a particular damage state occurs for different aftershock records after the same mainshock record (Fig 5.1(a,b)). However, when the mainshock records are different, but the aftershock record is same (Fig 5.1(c,d)), the building exhibits similar behavior in the aftershock. This observation illustrates that the history of the path to the mainshock damage state is less important than the level of the building damage. However, Fig. 5.1(d) shows more variability than Fig. 5.1(c), indicating that as damage states become more severe, the increasing nonlinear behavior increases the variation in structural response.

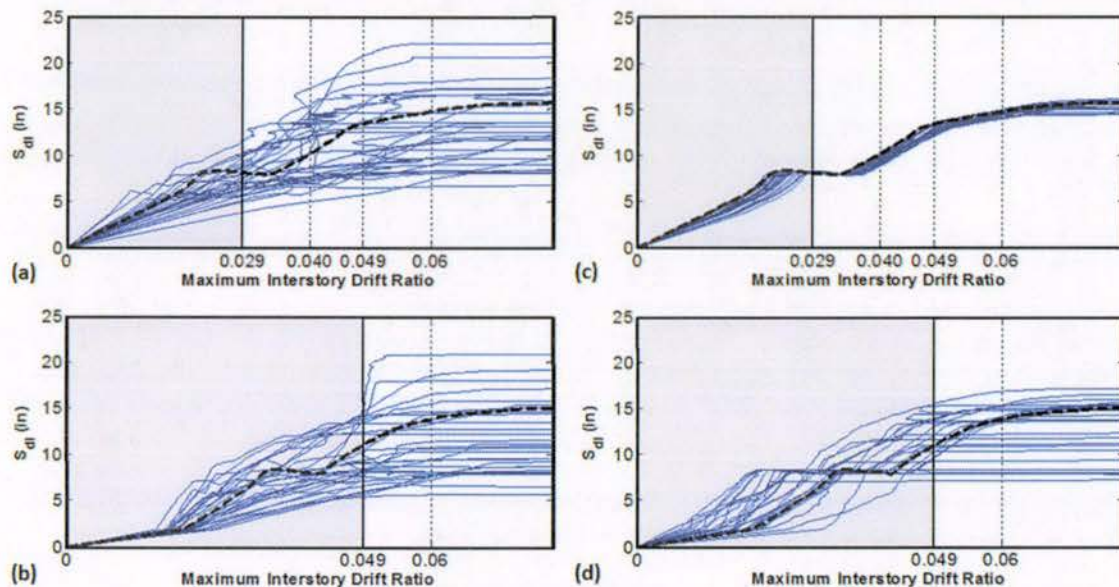


Figure 5.1 Incremental dynamic analysis results for the sequence where 30 different aftershock records were applied after experiencing either (a) moderate or (c) extensive damage in the same mainshock record; (b) and (d) show the behavior of the moderately and extensively damaged building, respectively, when subjected to sequences consisting of 30 different mainshock records, but the same aftershock record.

The dynamic analysis results from mainshock-aftershock sequences are used to compute the probability that a mainshock-damaged building will be in or exceed a particular damage state as a function of the aftershock shaking intensity (S_{dt}), as shown by the fragility curves in Fig 5.2. After the aftershock record, the building will either remain in the mainshock damage state or transition to a worse damage state (the building cannot become less damaged). Fragility curves can be computed using the relations obtained from Ryu et al. (2011). The fragility curves calculated for buildings with moderate, less extensive and extensive damage in the mainshock are shown in Fig 5.2 (a,b,c), respectively, and compared with the the damage state fragility curves for the intact building. Moderate damage (Fig 5.2(a)) does not significantly change a building's fragility to aftershock records. However, the difference in fragility between the damaged and intact buildings increases significantly for less extensively and extensively damaged buildings (Fig 5.2(b) and (c)). As the building becomes more damaged in the mainshock record, the standard deviation (or dispersion) in the aftershock fragility also increases, indicating greater record-to-record variability in response.

The polarity of the mainshock-aftershock ground motion sequence does not impact the post-earthquake fragilities for a moderately damaged building, but it can become noticeable for the extensively damaged building. During the fragility curve calculations, the polarity effect is explored

using positive, negative, random, and minimum polarity. The minimum polarity case uses IDA results from the ground motion sequence which causes collapse at the lowest S_{di} , considering both positive and negative polarities. The median capacity associated with the extensive damage state is found to be around 5% lesser using the minimum polarity compared to others. The results here correspond to the positive polarity of ground motions, but for future analysis, random polarity is recommended, since the polarity of future records is unknown.

Results shown in Fig. 5.3 indicate that the calibrated SDOF model shows reasonable agreement with the MDOF model, both in terms of prediction of the fragility of the intact structure and in prediction of the reduction in capacity due to damage in the mainshock. The SDOF reduces computational time by a factor of around 160.

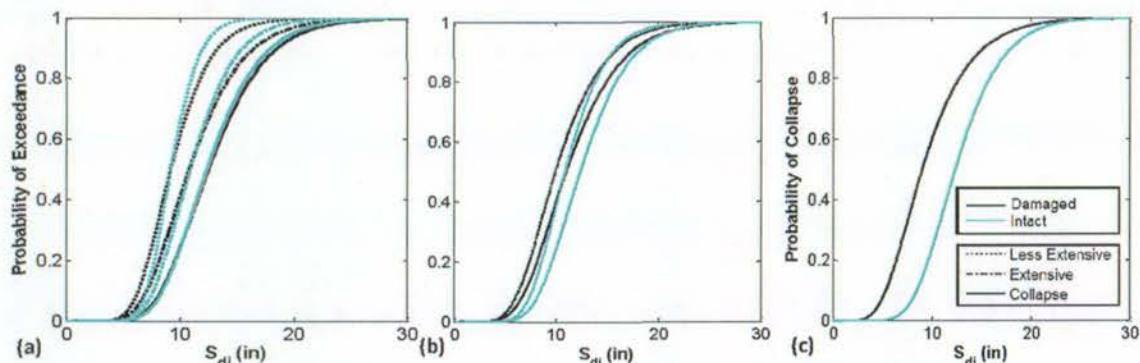


Figure 5.2 Fragility curves for building (a) moderately damaged in mainshock, (b) less extensively damaged in mainshock and (c) extensively damaged in mainshock (in black). The fragility curves for the undamaged (intact) building (blue) are shown for comparison.

To assess the performance of this non-ductile building during the 2010-2011 sequence of earthquakes in New Zealand, a nonlinear dynamic analysis is carried out on a set of recordings at 35 different sites in Canterbury from these two events (GeoNet, 2011a, 2011b). There are two horizontal components of ground motions recorded at each site for both the events, giving four possible earthquake sequences per site and, in total, 140 unique sequences. To consider the possibility that these independent events can occur in any order, 140 additional sequences are generated by reversing the order of two ground motions in the sequence. To explore the effects of stronger ground motions, all of the 280 sequences were multiplied by an arbitrary factor of 1.2, generating another set of 280 sequences. The damage state after the first event and the second event is observed and the transition probabilities between these events are illustrated in Fig. 5.4(a). Under the New Zealand sequences, the intact building is damaged to varying levels after the first event and, in some cases, further transitioned to a worse damage state after the second event. The median ground motion intensity associated with the onset of a particular damage state is calculated for the MDOF model subjected to New Zealand ground motions. These median capacities (called "New Zealand" results) are plotted in Fig. 5.4(b) along with the median capacities calculated for the MDOF subjected to the "general set" of records from Vamvatsikos and Cornell (2006). There is a decrease in the median capacity of the damaged building compared to the intact building on being subjected to New Zealand records, similar to what is observed for the general set of ground motions. On average, the median capacity of the structure using the New Zealand ground motions associated with each damage state is higher than for the general set, which may be due to different frequency content of the New Zealand ground motions. It is difficult to compare the damage seen in the actual New Zealand buildings during the earthquake sequences to the building damage in this study because the actual collapses occurred in buildings with different characteristics from our typical building. However, local failures similar to the extensive damage state were observed in a number of non-ductile buildings in New Zealand including beam-column joint failure, partial column failure etc. (EERI, 2011).

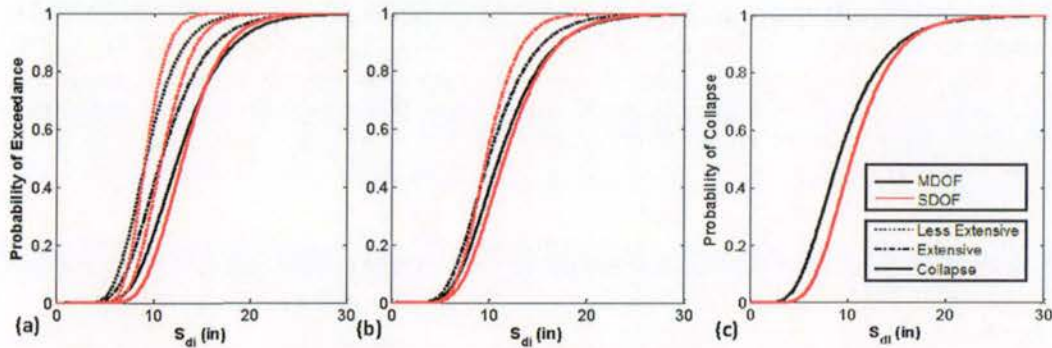


Figure 5.3 Fragility curves for SDOF model (red), when (a) moderately damaged in mainshock, (b) less extensively damaged in mainshock and (c) extensively damaged in mainshock. The fragility curves for the MDOF building (black) model are shown for comparison.

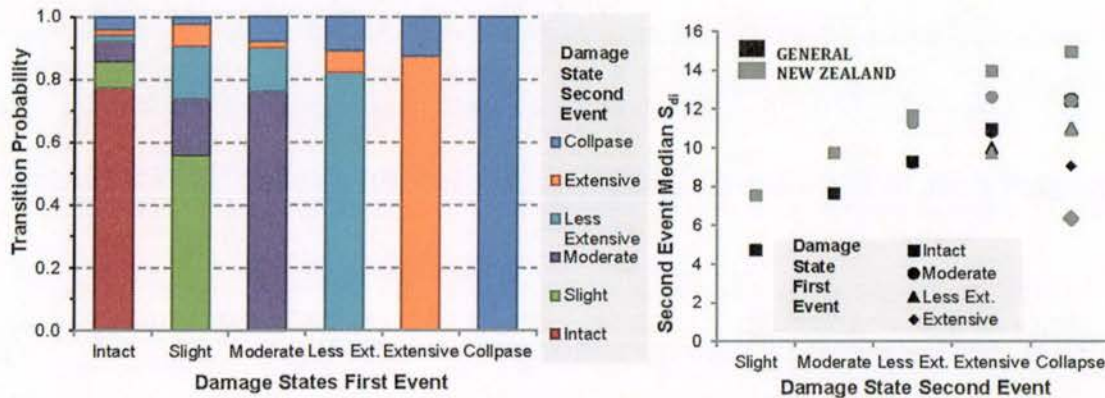


Figure 5.4 (a) Transition probabilities of the building from a particular damage state in first event to the damage state in second event for the New Zealand ground motions; (b) Comparison of the second event/aftershock median capacity for MDOF models using the general and New Zealand ground motions.

5. CONCLUSIONS

This study provides insight into the influence of earthquake sequences on building fragility. The moderately damaged building exhibits collapse capacity similar to an undamaged building, indicating that the building can be *green* tagged or in other words, is safe for use by its occupants. On the other hand, the building's ability to resist subsequent ground shaking decreases considerably when the structure is extensively damaged, and likely needs *red* tagging. The physical damage observed in the building during the extensive damage has description similar to the *red* tagged buildings in ATC-20, *i.e.* high interstory drifts, failure of any beam, column and joints hinges or local collapses. The results from a simplified SDOF system provides reasonable estimates median capacity of damaged and intact building, but exhibits lower standard deviation values because of less variability in damage propagation than a MDOF system. A similar analysis can be carried out on a suite of archetypical buildings prevalent in a region and building fragilities so computed for the intact and damaged buildings can be combined with the post-earthquake seismic hazard at site to prioritize regions for conducting post-earthquake inspections. These building curves also help to quantify the possible damage that may occur in buildings in a seismic region susceptible to multiple earthquakes from separate events.

ACKNOWLEDGEMENTS

Funding for this study comes from USGS cooperative agreement with the University of Colorado (Grant Number. G10AC00100). Conclusions and findings do not necessarily represent U.S. government policies.

REFERENCES

- Amadio, C., Fragiaco, M. and Rajgelj, S. (2003). The effects of repeated earthquake ground motions on the on-linear response of SDOF systems. *Earthquake engineering & structural dynamics*. **32**: 2, 291-308.
- ATC. (1989). ATC-20 Procedures for Postearthquake Safety Evaluation of Buildings. ATC
- ATC. (1995). ATC-20-2, Addendum to the ATC-20 Postearthquake Building Safety Evaluation Procedures. ATC
- EERI, 2011. Learning from Earthquakes -The M 6.3 Christchurch, New Zealand, Earthquake of February 22, 2011, EERI Special Earthquake Report.
- FEMA. (2009). Quantification of Building Seismic Performance Factors, FEMA.
- Frangiaco, M., Amadio, C. and Macorini, L. (2004). Seismic response of steel frames under repeated earthquake ground motions. *Engineering structures*. **26**: 13, 2021-2035.
- GeoNet. (2012a). Special processing for selected main-shock records from the Darfield Earthquake. ftp://ftp.geonet.org.nz/strong/processed/Proc/2010/09_Darfield_mainshock_extended_pass_band/
- GeoNet. (2012b). Special processing for selected main-shock records from the Christchurch Earthquake. ftp://ftp.geonet.org.nz/strong/processed/Proc/2011/02_Christchurch_mainshock_extended_pass_band/
- Haselton, C.B., Liel, A.B., Lange, S.T. and Deierlein, G.G. (2008). Beam-Column Element Model Calibrated for Predicting Flexural Response Leading to Global Collapse of RC Frame Buildings, PEER
- Hatzigeorgiou, G.D. (2010). Ductility demand spectra for multiple near-and far-fault earthquakes. *Soil Dynamics and Earthquake Engineering*. **30**: 4, 170-183.
- Hatzigeorgiou, G.D. and Beskos, D.E. (2009). Inelastic displacement ratios for SDOF structures subjected to repeated earthquakes. *Engineering Structures*. **31**:11, 2744-2755.
- Hatzigeorgiou, G.D. and Liolios, A.A. (2010). Nonlinear behavior of RC frames under repeated strong ground motions. *Soil Dynamics and Earthquake Engineering*. **30**: 10, 1010-1025.
- Ibarra, L.F., Medina, R.A. and Krawinkler, H. (2005). Hysteretic models that incorporate strength and stiffness deterioration. *Earthquake Engineering & Structural Dynamics*. **34**: 12, 1489-1511.
- Lee, K., Foutch, D.A. (2004). Performance evaluation of damaged steel frame buildings subjected to seismic loads. *Journal of Structural Engineering*, **130**: 4, 588-599.
- Li, Q. and Ellingwood, B.R. (2007). Performance evaluation and damage assessment of steel frame buildings under main shock-aftershock earthquake sequences. *Earthquake engineering & structural dynamics*, **36**: 3 405-427.
- Luco, N., Bazzurro, P. and Cornell, C. A. (2004). Dynamic versus static computation of the residual capacity of a mainshock-damaged building to withstand an aftershock. *13th World Conference on Earthquake Engineering*. Paper No. 2405
- OpenSees. (2012). "Open System for Earthquake Engineering Simulation. <http://opensees.berkeley.edu/>
- Ruiz-García, J., Moreno, J.Y. and Maldonado, I.A. (2008). Evaluation of existing Mexican highway bridges under mainshock-aftershock seismic sequences. *The 14th World Conference on Earthquake Engineering*. Paper 05-02-0090
- Ruiz-García, J. and Negrete-Manriquez, J.C. (2011). Evaluation of drift demands in existing steel frames under as-recorded far-field and near-fault mainshock-aftershock seismic sequences. *Engineering Structures*. **33**:2, 621-634.
- Ryu, H., Luco, N., Uma, S.R. and Liel, A. B. (2011). Developing fragilities for mainshock-damaged structures through incremental dynamic analysis. *9PCEE*. Vol. 225 1-8
- Smyrou, E., Tasiopoulou, P., Bal, İ.E., Gazetas, G. and Vintzileou, E. (2011). Structural and geotechnical aspects of the Christchurch (2011) and Darfield (2010) earthquakes In New Zealand. *Seventh National Conference on Earthquake Engineering*, Istanbul, Turkey.
- Sunasaka, Y. and Kiremidjian, A.S. (1993). A method for structural safety evaluation under mainshock-aftershock earthquake sequences, The John A. Blume Earthquake Engineering Center.
- Tothong, P. and Cornell, C. A. (2006). An empirical ground-motion attenuation relation for inelastic spectral displacement. *Bulletin of the Seismological Society of America*. **96**: 6, 2146-2164.
- USGS. (2012), United States Geological Survey. <http://www.usgs.gov/>.
- Vamvatsikos, D. and Cornell, C. A. (2006). Direct estimation of the seismic demand and capacity of oscillators with multi-linear static pushovers through IDA. *Earthquake Engineering & Structural Dynamics*. **35**: 9, 1097-1117.
- Vamvatsikos, D. and Cornell, C. A. (2002). Incremental dynamic analysis. *Earthquake Engineering Structural Dynamics*. **31** : 3, 491-514.



www.gns.cri.nz

Principal Location

1 Fairway Drive
Avalon
Lower Hutt 5010
PO Box 30368
Lower Hutt 5040
New Zealand
T +64-4-570 1444
F +64-4-570 4600

Other Locations

Dunedin Research Centre
764 Cumberland Street
Dunedin 9016
Private Bag 1930
Dunedin 9054
New Zealand
T +64-3-477 4050
F +64-3-477 5232

Wairakei Research Centre
114 Karetoto Road, RD4
Taupo 3384
Private Bag 2000
Taupo 3352
New Zealand
T +64-7-374 8211
F +64-7-374 8199

National Isotope Centre
30 Gracefield Road, Gracefield
Lower Hutt 5010
PO Box 31312
Lower Hutt 5040
New Zealand
T +64-4-570 1444
F +64-4-570 4657